Mechanisms of Focal Adhesions

Mayur Saxena

Submitted in partial fulfillment of the

requirements for the degree of

Doctor of Philosophy

in the Graduate School of Arts and Sciences

Columbia University

2018

Abstract

Mechanisms of Focal Adhesions

Mayur Saxena

Focal adhesions are dynamic multiprotein structures connecting cells to their surrounding microenvironment. Cells receive critical mechanical signals from adhesions that control many cellular processes including wound healing, differentiation, development, and cancer. Proteins that form adhesions are called adhesion proteins and some of these proteins can be mechanosensitive, meaning that they respond to mechanical stimuli. During spreading and migration, cells mechanically test extracellular matrix rigidity by contracting matrix to a constant displacement. Transmission and processing of such mechanical signals rely upon the dynamic regulation of the adhesions, which is tightly coordinated with activation of intracellular signaling cascades involving various adhesion molecules. However, the molecular mechanisms of mechanical signals that are transmitted through the adhesions to control cell behavior are poorly understood. In this thesis, we discovered novel phenomenon and mechanisms to elucidate roles of mechanical signals for multiple key aspects of basic cell behavior, especially cell growth.

We performed live cell imaging of cells spreading on fibronectin coated micropillars to understand adhesion formation, adhesion regulation, and their impact on cell behavior. One of the earliest molecules to arrive at an adhesion formation site is a mechanosensitive protein called talin which binds to several other entities to form the backbone of focal adhesions. We found a novel role of talin cleavage, which previously was thought to play a role only in focal adhesion turnover. We found that talin cleavage is a force dependent process that regulates proper adhesion formation, thereby governing several critical cellular processes. In the absence of this talin cleavage, cells formed abnormal adhesions and showed inhibited growth. Further, we found that upon inhibition of talin cleavage, one of the key cellular behaviors of increased cellular motility upon stimulation by epidermal growth factor seemed to disappear. Epidermal growth factor receptor is a transmembrane protein and has previously been shown to play important role in various cancers where cells exhibit altered rigidity sensing. Surprisingly, we found that epidermal growth factor receptor was required for cellular rigidity sensing only on rigid substrates, highlighting the importance of the interplay between mechanical and biochemical signals in determining cell behavior.

TABLE OF CONTENTS

List of Figures

Acknowledgements

I think I am a curious person and I enjoyed doing this PhD. Not just at the beginning, not just on the date of publishing, not just when I intend to finish it. I enjoyed doing this PhD throughout the process. The reason was Professor Michael Sheetz. He allowed and encouraged my curiosity. I still ask annoying (trivial) questions but I think I will always keep asking those annoying questions. The focus was always to frame a good question and then answer them, regardless of the methods at our disposal, regardless of whether or not it will lead to a publication. Another thing he taught me was to trust myself. Irrespective of how far away the results were from "general understanding" he taught me to trust the science. This learning for me goes way beyond this PhD. I am fortunate that I got Mike as my advisor.

I will also like to thank all my friends, colleagues and mentors and without their support this thesis would not be possible. Special thanks to everyone at Droice, who helped me at every point during my PhD and allowed me to actually finish this thesis.

It is tough to stay away from my family and from India. I did not know I will miss my family and India this much. Now I have a deeper desire to do something good for the world, especially my country.

Chapter 1

Introduction

1.1 Why does it matter?

Cells control and respond to mechanical forces from their microenvironment, which ultimately determines the final form of an organism. A number of key cell behaviors are affected by the interplay of external physical stimuli and cellular molecules to determine cellular shape, migration, proliferation, and apoptosis properties. The various biochemical mechanisms enabling cells to transduce mechanical stimuli into biological response collectively constitute mechanotransduction. At a molecular level, the underlying concept of mechanotransduction is that different molecules change their biochemical energy state upon application of mechanical forces. This change in biochemical energy can manifest in a number of cell-readable responses enabling the cell to "measure" the mechanical force. There are a number of mechanisms that enable this "measurement" by the cell, and one major hub of activity of such biophysical mechanisms is focal adhesions. Focal adhesions can be understood as biosensors that allow the cell to decipher physical signals like surrounding matrix stiffness or bio-mechanical properties of neighboring cells and then coordinate a number of cellular processes, including differentiation and growth. This communication between the cell and its microenvironment plays a critical role in a number of pathologies. For example, when certain cellular pathways (e.g., growth) are over- or under-stimulated it leads to disease conditions like fibrosis and cancer. Cells also continuously modulate their surrounding microenvironment by biomechanically assembling external protein structures.

For these reasons, understanding the underlying mechanisms of mechanotransduction is important. However, it is a challenge to quantitatively understand these mechanisms due to a wide variety of cellular processes that are affected by even a simple mechanical stimulus like force. Furthermore, most of the related literature from the last century is focused on establishing correlational connections by average cell or tissue expression levels. This has resulted in detailed molecular pathways involving hundreds of molecules. These pathways are extremely useful and helps us understand the key players involved in complex processes; however, these pathways fail to answer the question of *when* and *where* these molecular players interact.

In this thesis, we performed live cell imaging of cells spreading on fibronectin coated micropillars to understand the spatiotemporal dynamics of key molecules that affect adhesion formation, adhesion regulation, and their impact on cell behavior. In particular, we established a novel role of epidermal growth factor receptor (EGFR, a transmembrane receptor known to be involved in multiple cancers) in rigidity sensing of cells. By dynamically looking at EGFR we found it to be transiently interacting with focal adhesions and governing cellular mechanosensing. We also found that talin (a mechanosensitive protein connecting the integrins to the actin cytoskeleton) is cleaved at specific locations at particular points of time, an important phenomenon that was previously overlooked in adhesion formation.

Cells in the human body are subjected to continuously variable mechanical stimuli like force. It is understandable that the cellular response to these dynamic physical stimuli will

be dynamic. For example, if in a cancerous cell line, molecule A is overexpressed along with an adhesion molecule B, it is important to know if the two molecules interact. But it is even more important to understand when and where this event happens, because the mechanical microenvironment (for example, the surrounding substrate rigidity for a metastatic tumor) of this cell might vary drastically over time. It is plausible that molecule A localizes with molecule B only if the force is above a certain magnitude and a third independent molecule C is phosphorylated? In the future, effective medical interventions for diseases will be sophisticated combinations of chemical and physical methods. Thus, dynamic studies elucidating these biophysical pathways are the road to better medical interventions of tomorrow.

1.2 Focal adhesions are complex

Focal adhesions are dynamic protein structures connecting cells to their surrounding microenvironment. In particular, focal adhesions connect cells to the extracellular matrix through integrins and to actin cytoskeleton through a number of specialized proteins called adaptor proteins. There are several different types of adaptor molecules and together these form a hub of biochemical signal transduction and processing. Furthermore, because of this physical connection between the cell cytoskeleton and extracellular matrix, focal adhesions can relay small amounts of force in either direction, meaning that these structures are the physical location through which cells receive and respond to mechanical stimuli from the extracellular environment. Texture, mechanical rigidity, and force are all stimuli received by the cell. The cell's response (e.g., actin cytoskeleton contraction) results in forces applied by the cell on the extracellular matrix through focal adhesions. Further, focal

adhesions enable the cells to realize physical and topographical structures in cell's vicinity. As a result, the cell can then respond by modifying this extracellular space, or alter its contractility and migrate.

Focal adhesion assembly is a force-dependent process, meaning that focal adhesion growth increases with higher forces or higher substrate rigidity, while focal adhesions dissociate when these stimuli are removed. Hundreds of molecular players are involved in a coordinated process when forming this mechanosensitive structure. The exact mechanisms underlying the interplay between the molecules contributing to this mechanosensitive complex remain unclear, especially with respect to dynamic changes in focal adhesion structure caused by perturbations in mechanical stimuli. Focal adhesions consist of several mechanosensitive proteins like talin and vinculin determine focal adhesion behavior by responding to mechanical stimuli.

Due to a number of chemical, physiological, and mechanical entities that determine adhesion behavior, focal adhesions are complex. At any point of time in a live spreading cell, multiple factors – mechanosensitive proteins, substrate properties, cellular state, and several other cellular processes – are contributing to the cell's mechanosensitivity with the background of even more complex cellular pathways in different portions of the cell. Therefore, studying adhesions and mechanosensitivity is intrinsically difficult. In this thesis, we primarily use an early cell spreading model system to understand key mechanisms underlying adhesions and mechanosensitivity.

1.3 Early cell spreading model

When fibroblasts are allowed to spread on fibronectin coated glass at physiological temperature (37 °C), the cell usually spreads and polarizes within the first 40 minutes from the time of contact to the glass surface. Multiple studies in which suspended fibroblasts were seeded on fibronectin coated substrates revealed the same spreading behavior, where cells eventually polarized in a short span of 20-40 minutes. During this short period, the cell undergoes three main phases of behavior as a result of some key events involving the cellular mechanosensitive machinery, including initial adhesion formation, actin polymerization, myosin contractions along with changes in membrane tension, and rearward flow of actin. Therefore, if cells are seeded from a suspended state to the substrate and then imaged during the first few minutes, the following phases with clear physiological markers occur:

A/ Initial Attachment of the cell to the substrate – P0

B/ Rapid cell spreading, where the membrane reservoirs spread on the substrate – P1

C/ Slow cell spreading phase with protrusion/retraction cycles of the cell edge – P2

Since cells in experiments using early cell spreading models can be tracked right from suspension to maturing adhesions through checkpoints, the whole process ends up being highly reproducible, allowing quantitative studies of phenomenon that can be observed during early spreading. Since cell behavior is well established, there are very few confounding variables, and studies with high spatial and temporal resolution can be performed.

Adhesion assembly is a cell-microenvironment coordinated stepwise process in which the cell is organizing mechanosensitive protein tools to assess its microenvironment so as to respond appropriately via relevant signaling cascades. Adhesions start assembling as soon as the membrane comes in contact of the substrate, but they start to grow only when the cell starts to exert force on the substrate. As soon as adhesions start to grow, cells start mechanosensing, i.e., communicating with their surrounding microenvironment through these adhesions. Using this early cell spreading model, the process of adhesion formation and mechanosensing can be studied in very high quantitative detail.

1.4 Early Adhesion assembly

During P0, early adhesions assemble; one of the first steps in adhesion assembly is integrin clustering. Due to the multimeric nature of the involved proteins (leading to strong protein-protein interaction forces), integrin clustering provides stoichiometrically disproportionate increase in binding force when integrins bind to the matrix. These early integrins usually form near the cell periphery when the cell membrane protrudes away from the nucleus and fresh contacts with the extracellular matrix are formed. The underlying mechanism of this integrin clustering step is still unclear. However, it is understood that ligand binding to integrins transforms them into an activated state and the N-terminus of talin, a mechanosensitive protein, binds to the cytoplasmic portions of integrins during these early assembly events. Through its C-terminus, talin binds to the actin cytoskeleton. Once talin is connecting the actin cytoskeleton to the extracellular membrane in these early adhesions, actomyosin forces might be applied through these early adhesions on the attached substrate. Application of force is necessary for cells to be activated for further spreading as indicated

by the requirement of rigid barriers on lipid membranes for cells to proceed from P0 to P1. Therefore, even though the integrin activation step is force independent, there is a force dependent trigger step which "pushes" the cell for further spreading. Most of these early adhesions dissociate, but some adhesions under actomyosin force will develop into strong adhesion structures. If these actomyosin forces are blocked these early adhesions do not grow or mature. It is understood that the applied forces on early adhesions have to exceed a force threshold for adhesion reinforcement and growth.

1.5 Rapid spreading phase leading to rigidity sensing phase

Once the cell has made initial contact and integrin clustering and activation have occurred, the cell enters P1 phase marked by rapid actin polymerization resulting in the cell spreading out on the substrate. Interestingly this rapid cell area expansion is independent of actomyosin force and does not require any further integrin activation after P0. The cell expands until it depletes its membrane reservoirs, at the end of which the membrane tension peaks. This peak in tension can potentially signal for an increase in myosin-based contractility through a number of mechanisms involving hydrolysis of acidic phospholipids.

Once the membrane tension has peaked resulting in myosin activity, the cells begin to exhibit periodic contractions marking the beginning of P2 phase of spreading. These contractions, which result from controlled myosin activity, are involved in rigidity sensing. On rigid substrates, many more of these contractions or contractile units appear, whereas on a soft substrate, the number of these contractions is much lower and the cell spreading stops. It has been shown previously that cells try to stretch their substrate to a fixed

distance. This phenomenon is independent of the type of substrate and is observed on surfaces of varying rigidity (hundred-fold extension), type (continuous or pillars) and coating (integrin ligands). This strongly indicates that cells are estimating substrate rigidity by the force generated to achieve this constant substrate displacement.

Since rigidity sensing has been shown to be critical for multiple cellular pathways including differentiation and growth, several techniques have been used to understand the rigidity sensing mechanism, including traction force microscopy, laser tweezers, and pillar arrays. Previously, by using different pillar diameters, it has been shown that there are two unique contractile processes used by fibroblasts to sense substrate rigidity. The first is through the force applied on adhesions due to inward actin flow and the second is because of a 2-3 μm long contractile unit. When rigidity sensing was analyzed in fibroblasts on submicrometer diameter pillars, cells seem to displace the pillars to a constant distance of 50 nm, whereas when pillars with diameter greater than 1 μm were used, the pillar displacement seemed to scale with substrate stiffness. This constant displacement to 50 nm was a result of a of localized pairs of sub-micron diameter micropillars being displaced in opposite directions for a period of time (~25 s) forming the aforementioned contractile unit.

1.6 Talin and calpain mediated talin cleavage

One of the key molecules required for cell-matrix adhesion assembly is talin. Talin can bind to both integrins and F-actin. By binding to integrins, it can change the integrin's state from inactive to active. Once talin binds to both integrins and actin cytoskeleton, it creates a physically continuous system where forces can be transferred from actin cytoskeleton to

the substrate or vice versa. There are several other molecules that can potentially do the same, but the importance of talin was established through genetic studies. There are several organisms which express a well-conserved talin but do not express any integrin subunits, meaning that talin can perform functions without integrins, which is speculated to be possible through multiple signaling cascades not connected to integrins. Little is understood about talin's non-integrin associated functions but mutations in talin have been associated to a number of physiological conditions, like eye defects. Furthermore, when talin is knocked out in organisms, it leads to compromised phenotypes, including lack of adhesions, abnormal mechanosensing, and diminished cell viability.

By structure, talin is comprised of 2,540 amino acids with three key portions: the talin head, flexible linker, and talin rod. The talin head (residues 1-400) contains a FERM domain (F for 4.1 protein, E for ezrin, R for radixin, and M for moesin) that binds to the cytoplasmic domain of integrins. This region in talin also contains binding sites for phospholipids like PIP2, which is associated with establishing membrane tension. The talin head is connected to the talin rod through an unstructured region usually referred to as the flexible linker. The talin rod is the longest portion of talin, with multiple binding sites for actin, integrin, and vinculin, which in turn bind to several other protein partners.

There are multiple studies highlighting the role of talin in focal adhesion assembly and its role as a binding partner for several adhesion proteins. The flexible linker portion of talin has a site for cleavage by calpain2, a calcium ion dependent serine protease. Consequently, cleavage of talin in mature adhesions was shown to be critical for focal adhesion turnover and resulting loss of adhesion proteins like paxillin and zyxin from adhesion sites. Interestingly, although both talin and activated calpain2 are present during adhesion

formation, there is no literature on how and if talin cleavage affects adhesion formation or rigidity sensing.

Chapter 2

AIMS

2.1 General Aims

The aim of this thesis is to take a step forward in understanding the underlying mechanisms of focal adhesions and to decipher, both spatially and temporally, the organization, interaction, and effects of various cellular entities in direct or indirect response to a cell's microenvironment. Focal adhesions are a dynamic structure involving hundreds of proteins and affect critical cellular pathways for morphogenesis, growth, and differentiation, to name a few. This dynamic structure is continuously enabling the cell to communicate with its microenvironment and then respond appropriately. In this thesis, we aim to identify novel phenomenon involving some of the most well-known proteins involved in focal adhesions.

In particular:

In Chapter 3

We aim to identify if EGFR plays a role in rigidity sensing by the cell and how substrate rigidity can alter different EGFR activation pathways. This is critical since EGFR is involved in a number of disease conditions, including cancer.

In Chapter 4

We aim to identify if and how calpain mediated talin cleavage plays a role in adhesion formation, cell growth, and rigidity sensing. This is critical because talin is a mechanosensitive protein which forms the backbone of focal adhesions and changes to its state are connected to multiple key cell activities.

Chapter 3

The role of EGFR and HER2 in rigidity sensing through focal adhesion formation and development

Abstract

Epidermal growth factor receptor (EGFR) interacts with integrins during cell spreading and motility. However, little is known about EGFR's role in mechanosensing processes. Here, we show that EGFR or HER2 activity increases spreading and rigidity sensing contractions on rigid but not soft substrates without EGF or serum in two cell lines. Contractions peak after 15-20 min but diminish by 10-fold after 4 hours. Addition of EGF after 4 hours increases spreading and contractions, but myosin-II inhibition blocks this. Src family kinases (SFK) phosphorylate EGFR at nascent adhesions on stiff but not on soft substrates. Further, SFK inhibition or mutation of Src phosphorylation sites in EGFR or HER2 but not the EGFR autophosphorylation site mimics EGFR or HER2 inhibition. On soft surfaces, both EGFR inhibition and EGF stimulation didn't affect motility. Thus, EGFR or HER2 can catalyse rigidity sensing after associating with nascent adhesions under rigidity-dependent tension downstream of SFK activity.

Introduction

The rigidity of the extracellular matrix (ECM) plays a significant role in cell proliferation, differentiation, and motility[1–3]. During spreading and migration, cells mechanically test ECM rigidity by contracting matrix to a constant displacement[4]. If the force exceeds a threshold of about 25 pN during the displacement, early integrin adhesions are reinforced[5,6]. Recent studies show that these forces are generated through actomyosin-based sarcomere-like contractile units (CUs) producing nanometer-scale local displacements[6,7]. In addition, tropomyosin 2.1 (Tpm2.1), an important component of the local sarcomeric units, is a tumor suppressor required for anoikis on soft surfaces, reinforcing the idea that the early rigidity sensing process is critical for growth control[6]. AXL and ROR2 are tyrosine kinases that control sarcomeric unit displacement and duration, while AXL phosphorylates Tpm2.1 to catalyze adhesion assembly[8]. All this strongly supports the hypothesis that rigidity sensing is performed by the local sarcomeric contractions. Thus, analysis of the local CUs enables quantitative analysis of the level of rigidity sensing activity over extended time periods.

It is known that growth factor receptors interact with integrins during cell spreading and migration[9–11]. Previous studies have shown that upon acute EGF stimulation, EGFR activates spreading and myosin II contraction, leading to focal adhesion (FA) redistribution[12,13]. In the absence of EGF, EGFR also regulates cellular functions like proliferation and cell cycle control by activation in an adhesion-dependent, ligand-independent manner. Interplay between EGFR and its other isoforms like HER2 has previously been shown to play important role in several cancers[14] where cellular rigidity sensing is altered. Further, there is a strong link between EGFR and contractility through

phospholipase C (PLC) and the activation of protein kinase C (PKC)[15]. At an upstream level, active SFKs are recruited to early integrin adhesions, and in biochemical assays SFKs phosphorylate and activate EGFR[9]. Together, EGFR and the cells' underlying substrate appear to be involved in cellular motility and traction forces. Because rigidity sensing is a fundamental activity during cell spreading and migration, we conjecture that EGFR activation may affect rigidity sensing activity and early adhesion site formation (focal complexes that are localized at cell periphery[16,17]).

We analyzed the level of rigidity sensing events in spreading cells as a function of ligand independent EGFR activity. Surprisingly, EGFR activity was necessary for rigidity sensing on stiff but not on soft surfaces. Further, we found that EGFR activation of rigidity sensing depended upon myosin contractile activity. Thus, EGFR is involved in a positive feedback control of adhesion formation on rigid fibronectin surfaces but is much less active on soft surfaces. These results are consistent with the hypothesis that stretching of an early component in adhesion complexes recruits EGFR that then catalyzes rigidity sensing. Interestingly, we found that the lack of rigidity sensing in the absence/inhibition of EGFR on stiff substrates could be rescued by overexpression of HER2 – the latter having previously been correlated to a variety of cancers[18] - in a Src kinase dependent manner.

Results

Density of local contractile units peaks at early spreading

Previous studies showed that fibroblasts apply local contraction forces to substrates to test their rigidity through local actomyosin-based contractile units (CUs)[5,6]. Cells were plated on 0.5 μm diameter Polydimethylsiloxane (PDMS) pillars coated with fibronectin (FN) and displacements were tracked in real-time to detect CUs (Fig. 1a). Each rigidity-sensing event was dynamic and transient. One cycle of pulling and release typically lasted 20-40 seconds (Fig. 1b) and was located 1-3 μm from an extending cell edge (Fig. 1a). The previous studies of these CUs focused on early spreading (~30 min)[5,6] but not longer durations. To extend the time range of the measurements, we developed an automated program to measure pillar deflection and identify CUs (see Methods).

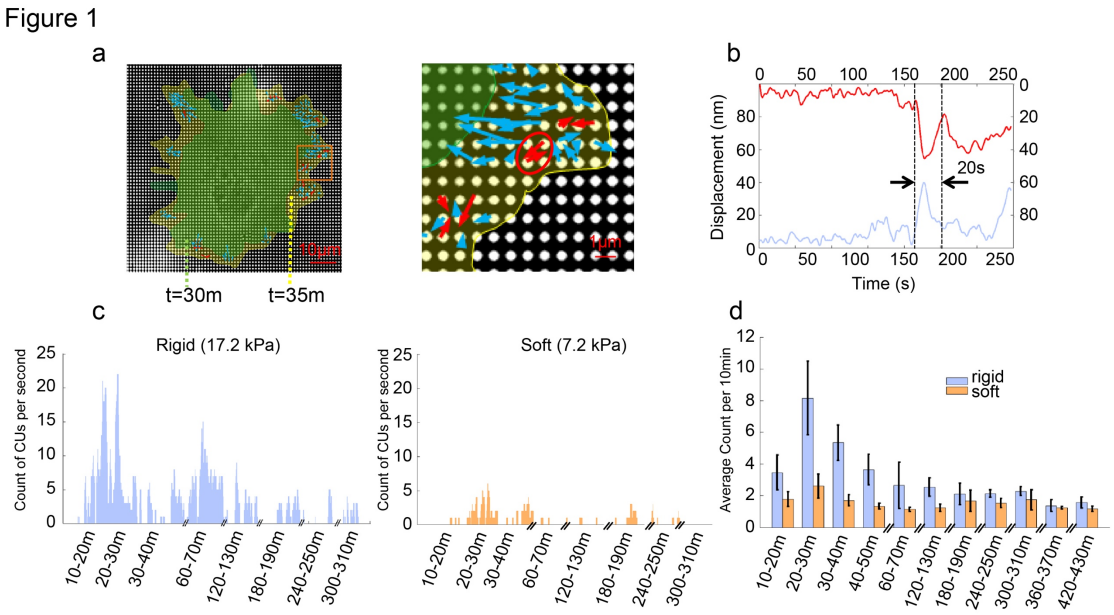

Figure 1 Rigidity sensing activity measured by local CUs number. **a**, actual CUs observed at the outward extending edge of a cell spreading on FN-coated 17.2 kPa pillars. Arrows represent pillar movement: red, detected CUs; blue, non-CUs. The red circles marks an

example of correctly identified CU. Cell edges marked in green and yellow correspond to time points 30 and 35 minutes respectively. **b**, displacement vs. time of two 0.5 µm pillars (red and blue curve) that composed a CU (circled in a). The dotted lines mark the beginning and end time point of the CU. Measurement of CUs per entire cell per second for rigid (**c**) and soft (**d**) pillars. Cells were plated on FN-coated pillar substrate in media lacking serum for over 7 h. **e**, average number of CUs per 10 min for cells on two pillar substrates of different stiffness in media lacking serum. n>10 cells per condition. n>5 independent experiments. Error bars show standard error of the mean.

CUs formed at a relatively constant density in lamellipodial extensions of the cell edge (active areas) but not in stationary regions (static areas; Supplementary Fig. 1a,b). After the initial burst of contractile activity in spreading, the number of CUs dropped dramatically. Thus, there was a strong correlation between the level of spreading activity and CU activity in control cells (Supplementary Fig. 1c).

Supplementary Figure 1

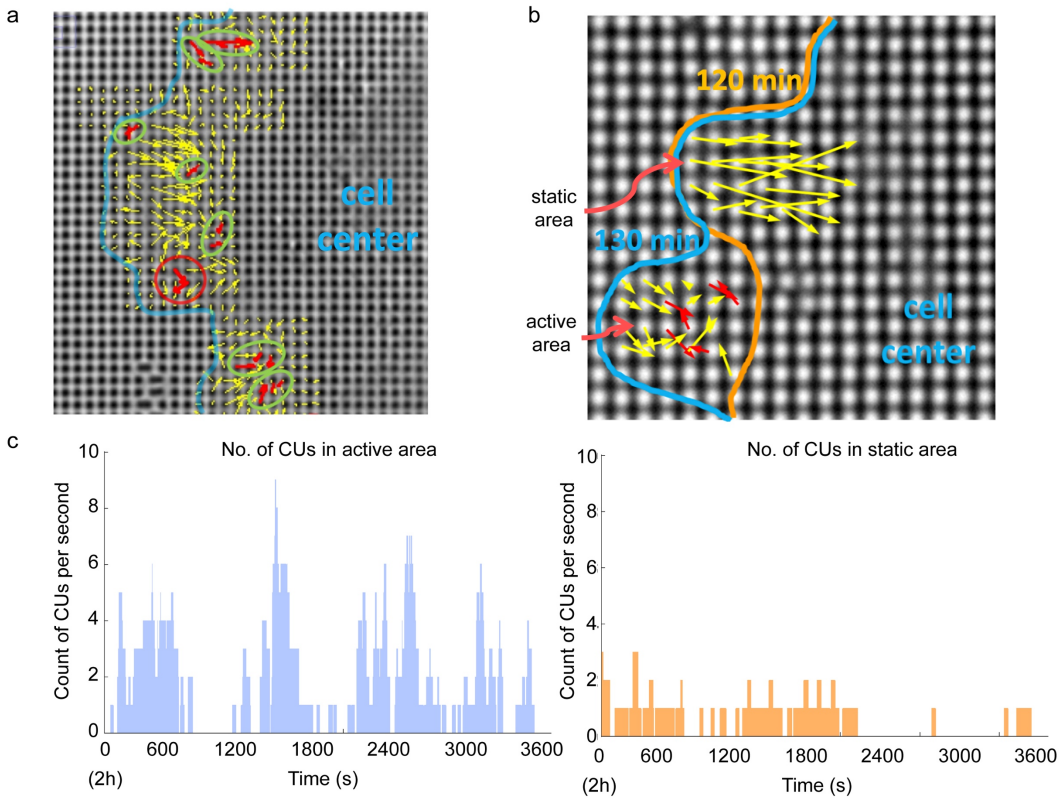

Supplementary Figure 1 CUs detection method and definition of active area. **a,** actual CUs detected in the active area by the automated program. Shown is a frame from a time-lapse movie of a cell spreading on FN-coated 17.2 kPa pillars. Arrows represent pillar movement: red, detected CUs; yellow, non-CUs. Green circles marked correctly identified CU; red circle marked incorrectly detected CU. Success rate=97.47+/-0.75%. Cell edge marked in blue. **b,** cell edge marked in orange and blue correspond to time 120 min and 130 min respectively. Active area is defined as the area where the cell edge moves outwards. **c,** number of CUs per second of the cell in **b** monitored from 2h to 3h**.** The left and the right plots show the number of CUs in the active and static area, respectively.

When cells were plated on a relatively stiff pillar matrix (bending stiffness = 6 nN/μm, effective modulus = 17.2 kPa, see Methods for calculation), the number of contractile units per cell peaked at ~20 minutes after binding (Fig. 1c). CU activity decreased by about ten-fold in 5 hours and remained low. The peak of CU density in early spreading coincided with the contractile spreading phase P2[19], in which cells tested substrate rigidity by local CUs across their edges[5,6]. After 30-60 minutes of spreading, cell edges were relatively stable; however, small areas moved outward periodically about every 5 minutes on average and those occasioned 5 or more CUs. Thus, the density of CUs was greatest in early spreading, although the cell continued to test the surface rigidity intermittently.

Next, we followed CU activity on soft pillars (effective stiffness=2.5 nN/μm, effective modulus=7.2 kPa) over long time periods (Fig. 1d). On these pillars, cells exhibited a lower level of rigidity sensing activity, evidenced by overall lower CU density (Fig. 1e). Again, occasional extensions activated CUs but those were typically followed by edge retractions giving cycles of extension and retraction over 20-40 minutes. These data were consistent with previous findings that adhesion complexes dissociated due to insufficient force for reinforcement on soft substrates[6].

Ligand-free EGFR activity is necessary for rigidity sensing

Since integrins cooperate with EGFRs in regulating cellular interactions with the extracellular environment[20] and co-clustered with FAK[21], we tested the role of EGFR kinase activity in CU activity during spreading. Previous evidence of integrin-EGFR complexes residing in immature FAs rather than mature FAs[22], indicated that ligand-independent EGFR activation could play an important role in regulating rigidity sensing

Figure 2

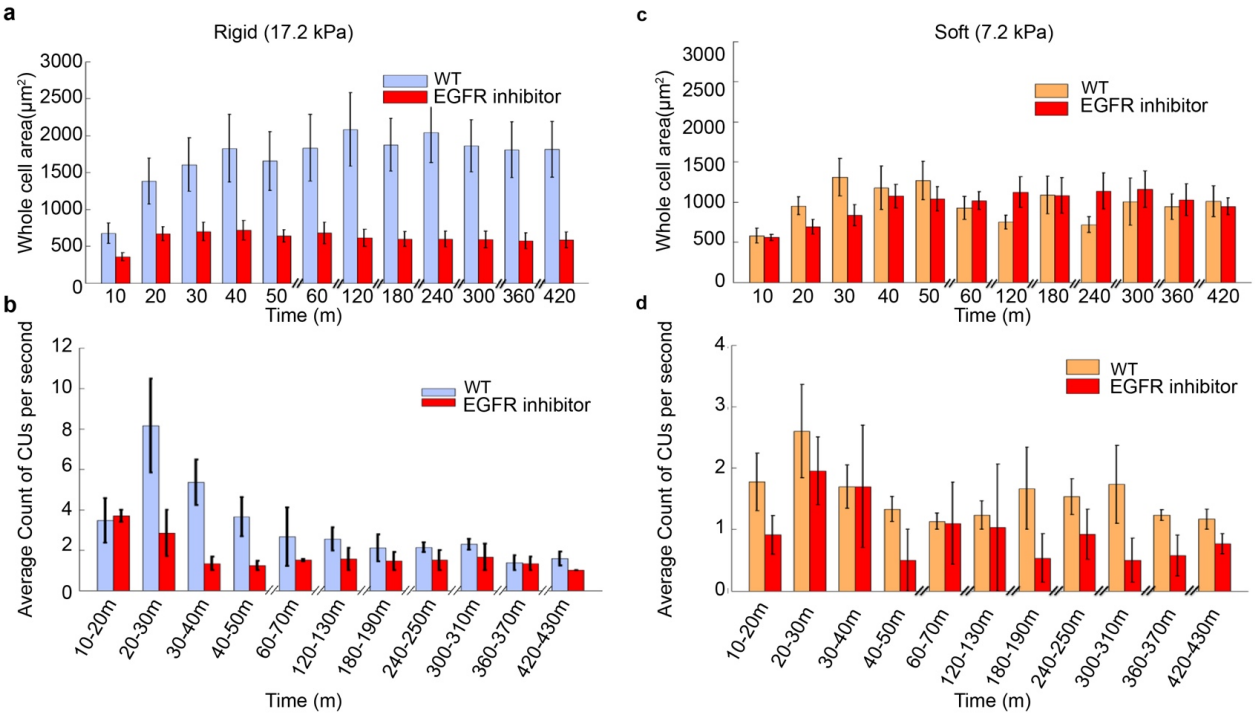

Figure 2 Ligand-free EGFR and HER2 activity affects local CUs **a** and **c,** increment of cell area normalized to initial size with respect to time. Cells were plated on FN-coated stiff (**a**) and soft (**c**) pillar substrates in serum-free medium with and without 10 nM EGFR inhibitor gefitinib (n≥10 cells for each condition, n>5 independent experiments). **b** and **d,** average of number of CUs per second for 10 min windows monitored for 7 hours on stiff (**b**) and soft (**d**). Error bars show standard error of the mean in all cases.

during early adhesion formation. When cells were plated on FN-coated pillar substrates, in medium lacking serum (growth factors) with EGFR inhibitor, they spread abnormally.

Initially, on stiff pillars, EGFR inhibitor caused slower spreading and cells reached normal P1 areas (the rapid spreading phase without contractions) typically only after ~20 minutes (compared to normal times of ~3-10 minutes). However, they failed to spread further (Fig. 2a), exhibited a much smaller active area (Supplementary Fig. 2a), and had very few CUs (Fig. 2b). These cells often adopted a dendritic morphology and had narrow extensions instead of broad lamellipodia (Supplementary Fig. 2b). On soft pillars, EGFR inhibitor was

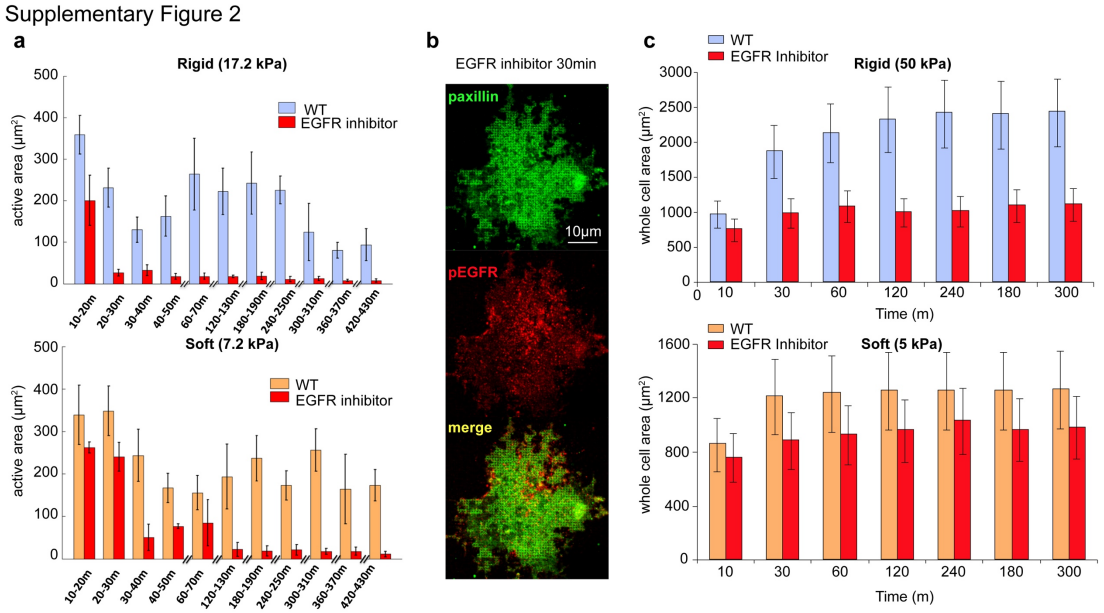

Supplementary Figure 2 Active area and pEGFR distribution disrupted by EGFR inhibitor and whole cell area on FN coated flat PDMS substrates. **a,** active area was measured in intervals of 10 minutes. Cells with and without EGFR inhibitor treatment in medium lacking serum were monitored on rigid (top panel) and soft (bottom panel) pillar substrates for over 7 hours. **b,** phosphorylated EGFR lost co-localization with paxillin with EGFR inhibitor (gefitinib, 10 nM) treatment on rigid pillar substrate. **c,** Whole cell area of

WT MEFs when spread on FN coated soft and stiff flat PDMS substrate with or without EGFR inhibitor. Error bars show standard error of the mean.

ineffective. Cells spread to a similar overall area and had a similar average CU density with or without inhibitor (Fig 2c,d). We verified that cells on continuous FN-coated gels of rigidity 5.5 kPa and 50 kPa showed the same rigidity dependence of EGFR inhibition as cells on the pillars (Supplementary Fig. 2c). Thus, the spreading and contractile activity of cells dramatically decreased after EGFR inhibition on rigid but not on soft surfaces.

To confirm that EGFR was the specific isoform involved and not the other ErbB isoforms (ErbB2/3/4), we analyzed cos-7 cells, which primarily express ErbB1/EGFR (to enable

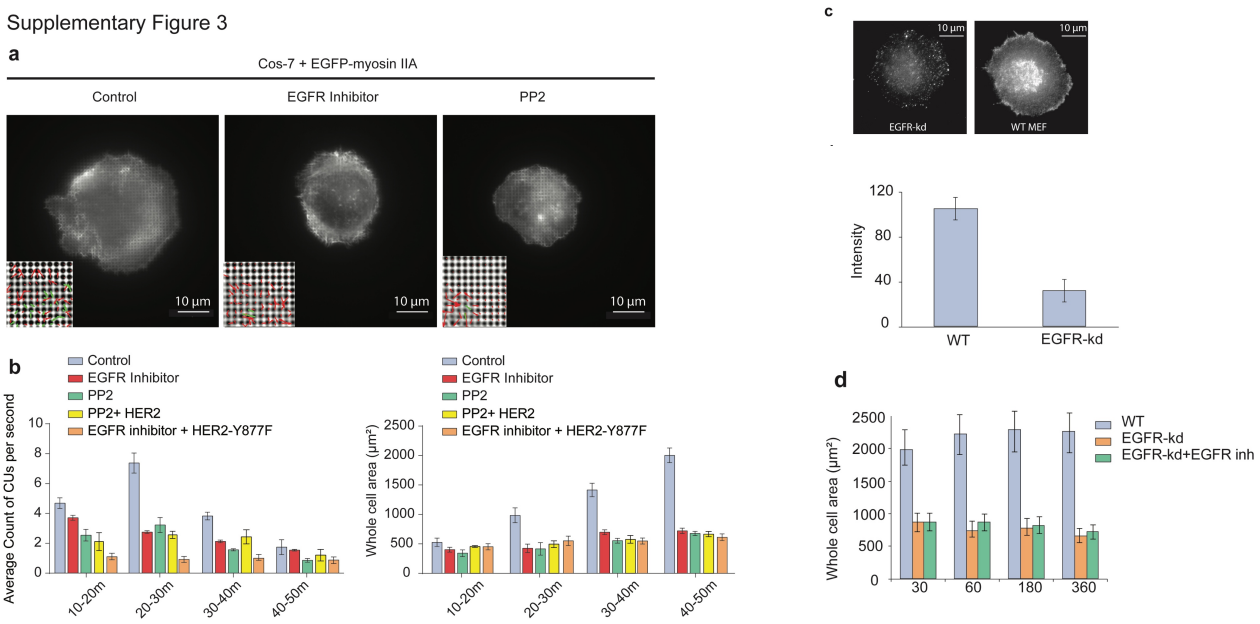

Supplementary Figure 3 Confirmation of EGFR and HER2 involvement in Cos-7 and WT MEFs using small molecule inhibitors and inactive HER2 point mutant. **a,** Cos-7 cells expressing myosin IIA were spread on rigid pillars with or without EGFR and/or HER2

inhibitor or PP2**.** Further, Cos-7 cells were transfected with HER2 mutant (Y877F) in combination with the mentioned inhibitors. The arrows in the inset show pillar displacements. **b**, Whole cell area and contractile unit count for the first hour of spreading. **c,** WT MEFs and cells with knock-down of EGFR stained for total EGFR. Average total intensity is also shown to signify the extent of knock-down. 22 cells were analyzed for each case. **d,** Whole cell area of EGFR knock-down cells as a function of time. 18 cells were analyzed from 3 independent experiments. Error bars show standard error of the mean.

cos-7s to form rigidity-sensing CUs, they were transfected with myosin-IIA, which is needed for mechanosensing[23] but is not expressed in cos-7s). As expected, EGFR inhibitor significantly reduced CU formation and spreading area of cos-7s on rigid pillars

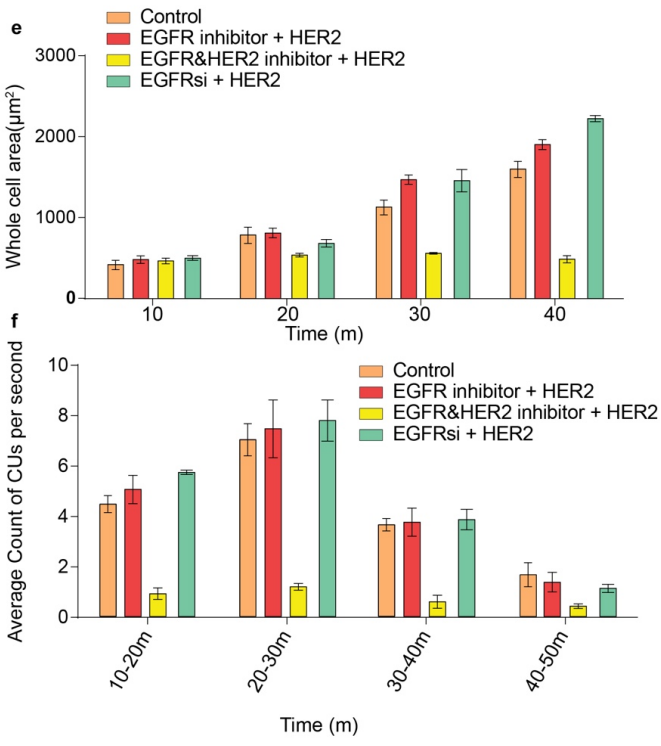

Fig. 2 contd. e, Cos-7 cells expressing myosin IIA were transfected with the HER2 plasmid and then spread on stiff pillars in the presence or absence of EGFR inhibitor, EGFR+HER2 inhibitor or HER2 siRNA. **f**, Average number of CUs per second in 10 minute windows for cells in **e**. Error bars show standard error of the mean in all cases.

Both MEFs and cos-7 cells express low levels of ErbB2 (HER2) and endogenous HER2 does not seem to support contractile activity. However, HER2 is a ligand independent EGFR family receptor sharing several downstream targets with EGFR[14,24]. When HER2 was overexpressed in cos-7 cells (expressing myosin-IIA), EGFR inhibition had no effect on CU activity and spreading area (Fig. 2e,f). However, addition of a small molecule inhibitor for both EGFR and HER2 caused a significant drop in CUs and spreading area, similar to EGFR inhibition of wild-type (WT) cells (Fig. 2a,b). To confirm this rescue, we knocked-down EGFR expression in cos-7s (expressing myosin-IIA) and then overexpressed HER2. Again, these cells had fully restored contractile activity and normal cellular spreading (Fig. 2e,f). Thus, under normal conditions EGFR that is involved in the mechanosensing process and there is not enough HER2 to contribute, but HER2 overexpression can replace EGFR function.

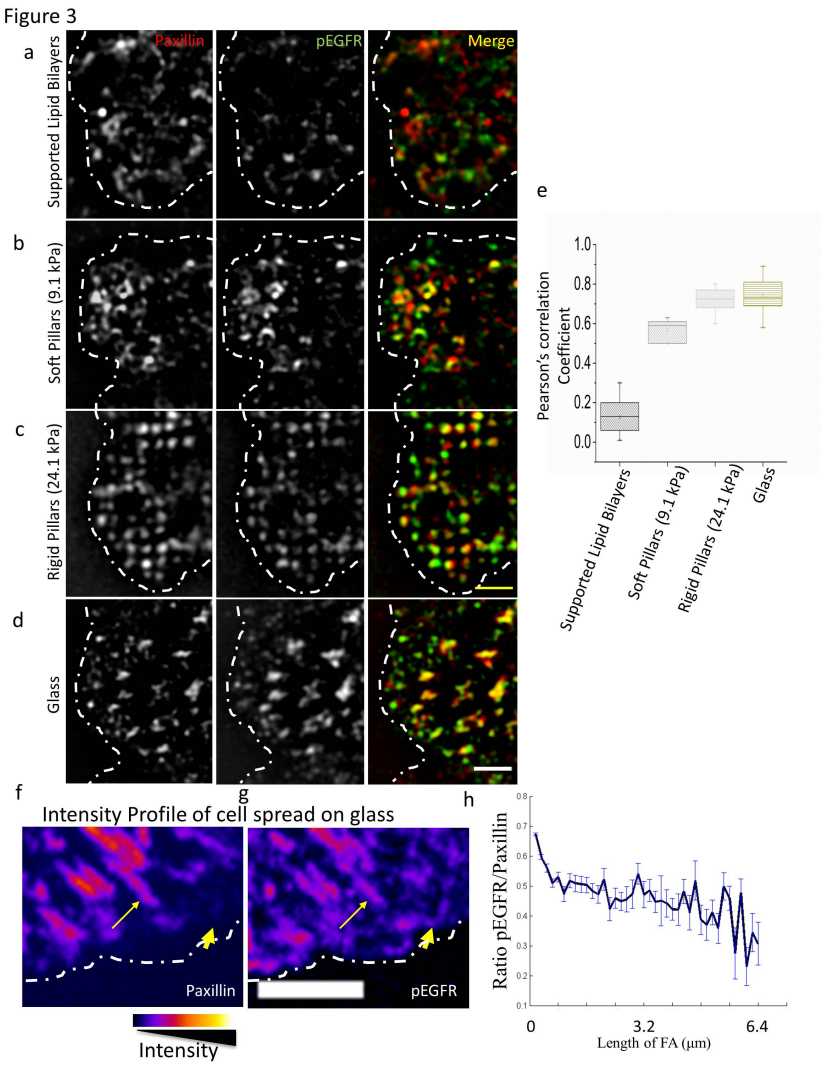

Figure 3 pEGFR localizes to early adhesions on rigid substrates. **a-d,** A region of MEF-WT spread on Supported lipid bilayers (15 minutes), soft (7.2 kPa) or rigid Pillars (17.2 kPa; 25 minutes), or on glass (10 minutes), stained with paxillin (red) and pEGFR (Y1068, green), and imaged using structured illumination microscopy. Dotted white line marks the cell boundary. Scale bar is 2μm. **e,** Pearson's correlation coefficient measured in the cells spread on different substrates between Paxillin and pEGFR. 30>n>10. For cell spread on pillars, colocalization was analyzed on a set of 6-8 pillars near the leading edge of the cell. **f-g,** Pseudo color images taken with confocal microscope (scale shown below) of MEF-

WT spread on glass stained with Paxillin (**f**) and pEGFR (1068; **g**). Dotted line marks the cell boundary. Thick arrows mark localization to early adhesions and thin arrows mark localization to maturing adhesions. Scale bar is 5 μm. **h** Ratio of pEGFR intensity to paxillin intensity in adhesions of increasing size. Error bars show standard error of the mean.

Src mediated ligand-independent activation of EGFR

In the absence of ligand, EGFR or HER2 could be activated by Src[25]. To test this in our system, we performed cross-correlation analyses on super-resolution structured illumination microscopy (SIM) images of active phospho-EGFR with paxillin in adhesion sites after immunostaining with an antibody that reacted with a Src-dependent phosphorylation site on EGFR (Y1068). Besides the two aforementioned pillar arrays, we performed these experiments on two substrate extremes: glass coated with RGD ligands (stiff), and lipid bilayers in which RGD ligands diffuse freely (without force) (Fig. 3a-e). We found that paxillin adhesions were not associated with pEGFR on lipid bilayers (Fig. 3a), but on glass pEGFR colocalized with paxillin (confirmed by Pearson's correlation coefficients (Fig. 3e)). In many cases on RGD coated glass, pEGFR was found in nascent adhesions before paxillin recruitment and as adhesions matured the pEGFR/paxillin ratio decreased (Fig. 3f,h). As a control, we stained WT cells with an antibody that reacted with the Src-independent EGFR autophosphorylation site (Y1173) and found a general staining of the cell surface, with no specific localization to active cell edges (Supplementary Fig. 4a,b). These results were further confirmed by measuring the intensity ratio at the cell edge compared to inner cellular locations (Supplementary Fig. 4a) of pY1068 EGFR as well as

another Src-dependent phosphorylation site on EGFR (Y845) on stiff and soft pillars (Supplementary Fig. 4c,d).

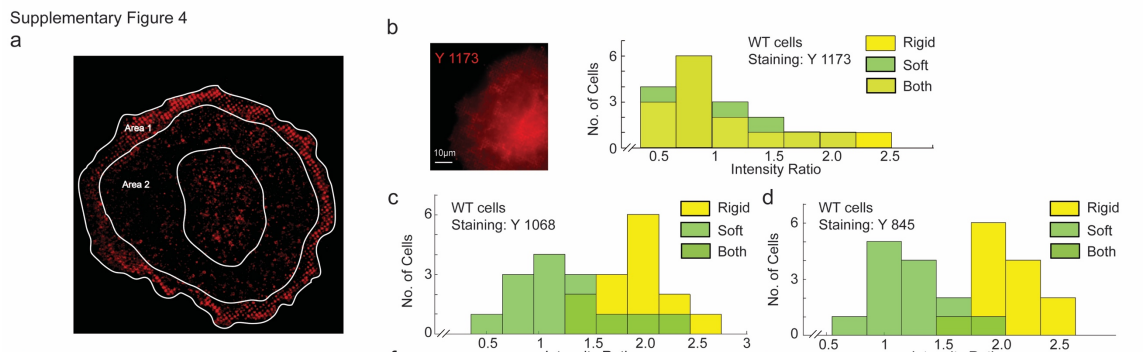

Supplementary Figure 4 Quantification of pEGFR distribution at cells edges. **a,** Average Intensity of pEGFR was calculated in Area 1 and Area 2 as shown. Area 1 is defined as a band across the cell edge with a width of ~4-5 μm. Intensity ratio is calculated by dividing the mentioned average from Area 1 by that of Area 2. This calculated Intensity ratio is a measure of the peripheral localization of pEGFR. In the following plots intensity ratio is plotted for the mentioned cells on stiff and soft substrates. **b,** WT cells stained for pEGFR Y1173. **c,** WT cells stained for pEGFR Y1068. **d,** WT cells stained for pEGFR Y845.

Also, inhibition of EGFR kinase activity on stiff pillars blocked paxillin and pEGFR co-localization (Supplementary Fig. 2b). Thus, Src-activated EGFR colocalized with integrin clusters at peripheral adhesions only when they were under force.

SFK activation of EGFR is required for rigidity sensing

Since EGFR inhibition was effective on stiff but not on soft pillars, and EGFR activation through Src was force-dependent, we hypothesized that Src-dependent activation of EGFR

was required for rigidity sensing. Inhibiting Src activity with PP2 (at concentrations that blocked only Src kinases and not EGFR [100-200 nM]) caused a significant decrease in the level of local CU activity, active edges, and spread areas in MEFs (Fig. 4a-c, Supplementary Fig. 5a) as well as in cos-7 cells (Supplementary Fig. 3a,b). To confirm the role of Src-dependent phosphorylation of EGFR, we mutated the Src-dependent phosphorylation site, Y845F or the autophosphorylation site, Y1045F) and expressed in EGFR (Fig 4c,d). Further, both PP2 addition (Supplementary Fig. 3b) and mutation of the Src phosphorylation site in HER2, Y877F, blocked the ability of HER2 to restore spreading and rigidity sensing in cos-7 cells after EGFR-kd or inhibition (Fig. 4c and Supplementary Fig. 3b). Thus, we suggest that both EGFR and HER2 are activated by SFK activity on rigid surfaces.

To determine which Src kinase was involved, we studied SYF cells that lack major SFKs (Src, Yes and Fyn), and found that pEGFR did not co-localize with paxillin at peripheral

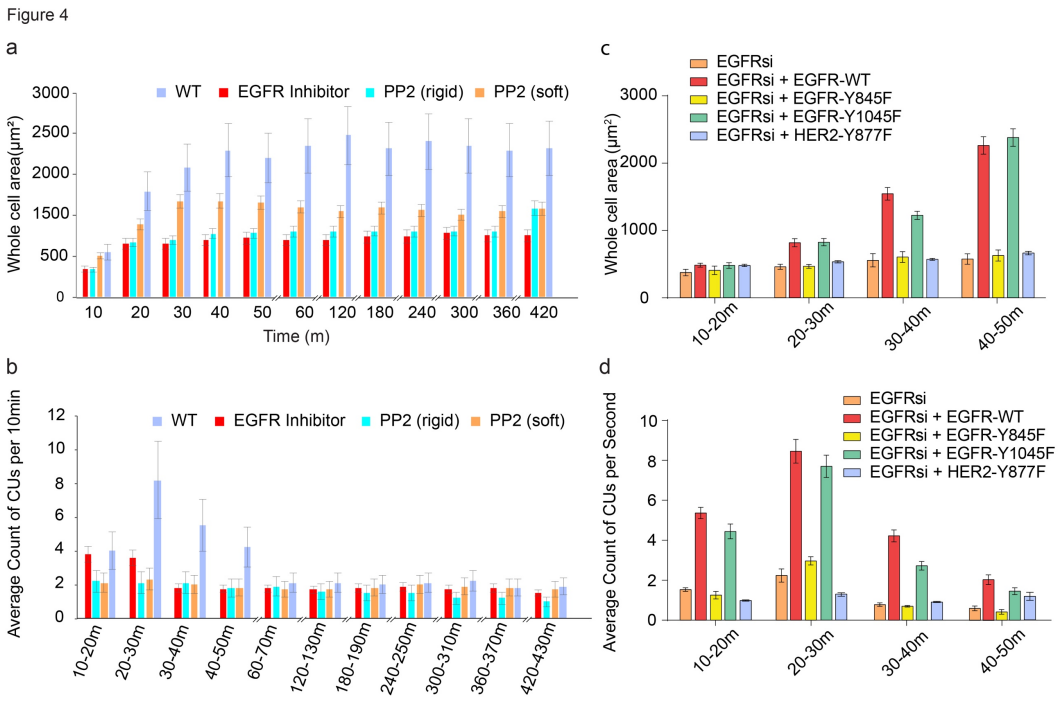

Figure 4 EGFR and HER2 affect local contractility through Src. **a**, cell area with respect to time. Cells were pre-incubated with PP2 (200 nM) for 30 min prior to plating on FN-coated pillar substrates in serum-free medium. n>15 cells, n>5 independent experiments. **b,** Average of CUs number per 10 min monitored for 7 hours. **c**, Cell area of Cos-7 cells expressing myosin IIA when transfected with siRNA for EGFR and variations of EGFR or HER2 on FN coated stiff pillars. **d**, Average number of CUs in 10 minute windows for the cells shown in **c**. Error bars show standard error of the mean.

adhesion sites (Supplementary Fig. 4e, Supplementary Fig. 5b,c). With stable knock-ins of c-Src, c-Yes or Fyn in SYF cells[26], we found that any of the knock-ins restored colocalization of pEGFR with paxillin (Supplementary Fig. 4f, Supplementary Fig. 5b,c).

Thus, these data indicated that SFK-dependent EGFR or HER2 tyrosine kinase activity played a critical role in promoting rigidity sensing and cell spreading on stiff matrices.

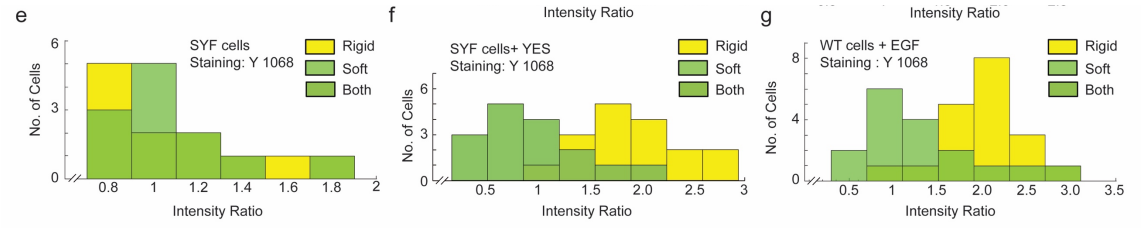

Supplementary Fig. 4 contd. e, SYF cells stained for pEGFR Y1068. **f,** SYF stably expressing YES stained for pEGFR Y1068. **g,** WT cells stimulated with EGF and then stained for pEGFR Y1068.

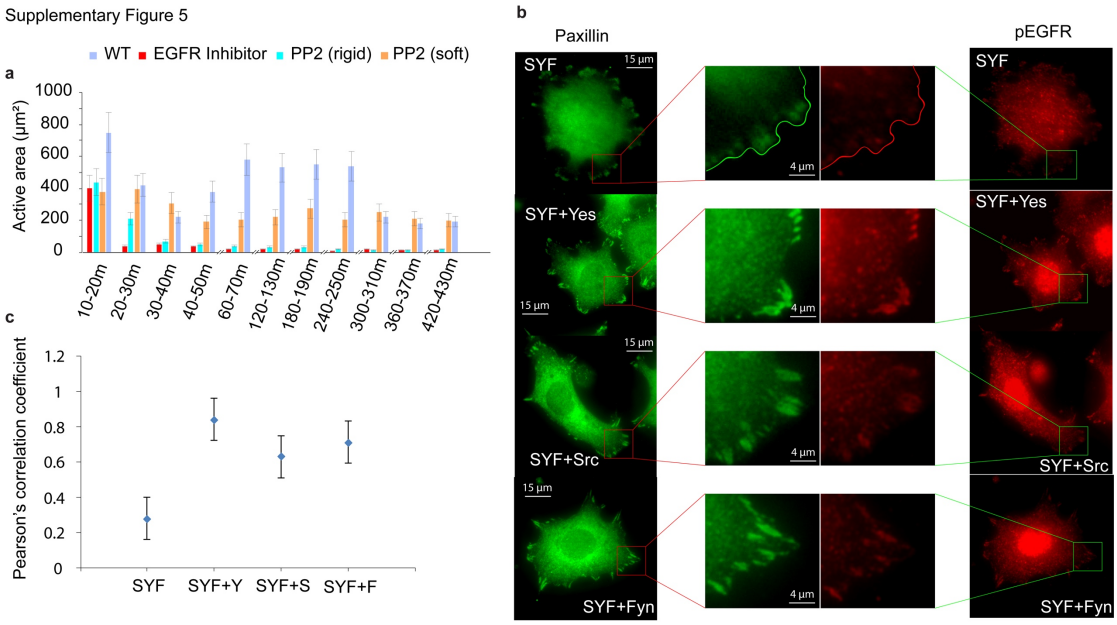

Supplementary Figure 5 Establishing the connection between SFKs and EGFR in cell spreading and adhesions. **a,** Active area of WT MEFs on stiff and soft pillars, with or without PP2. **b,** SYF cells and respective knock ins stained for Paxillin and pEGFR after 30 min of spreading on glass. **c,** Pearson correlation coefficient between paxillin and pEGFR in peripheral zone of cells as defined by Area 1 in Supplementary Figure 4a. n>10. 3 independent experiments. Error bars represent standard error of the mean.

EGF stimulates an increase in rigidity sensing on rigid surfaces

EGF is known to promote cell migration and growth through increased force generation and adhesion formation[27]. Evidence has shown that acute EGF stimulation causes phosphorylation of myosin regulatory light chain (MRLC) to promote myosin-II contraction[15], nearly simultaneously with adhesion assembly and paxillin phosphorylation in the adhesions[13]. Together, direct observations of focal adhesion assembly in cell

protrusion areas and increased contraction force induced by acute EGF stimulation[13] led us to hypothesize that EGF also had an effect on local contractile forces that sense rigidity.

To test if EGF stimulated rigidity sensing, we added 100 ng/ml EGF after 6 hours of cell adhesion to FN-coated stiff pillar substrates (17.2 kPa). A large portion of the cell edge moved out ~2 minutes after EGF addition, increasing cell area (Fig. 5a). After ~15 minutes, the lamellipodia retracted in a large fraction of cells (Supplementary Fig. 6a), rapidly recovering pre-EGF area levels (Fig. 5c). Further, EGF addition caused a dramatic increase in CU number in extending regions (Fig. 5b). At ~2 minutes after EGF addition, CU density increased dramatically to the levels seen at 15-20 min of spreading (Fig. 5d), and remained at this level for about 10-20 minutes before returning to the basal level after an additional 30 minutes. During the peak of EGF stimulation, local contractile force reached ~30% of total cell contraction force in the extending areas (Supplementary Fig. 6b). These activation events were blocked by EGFR inhibitor (Fig. 5d, Supplementary Fig. 6c). Thus, on rigid surfaces, EGF activates cell spreading and CU formation through kinase activation.

Figure 5

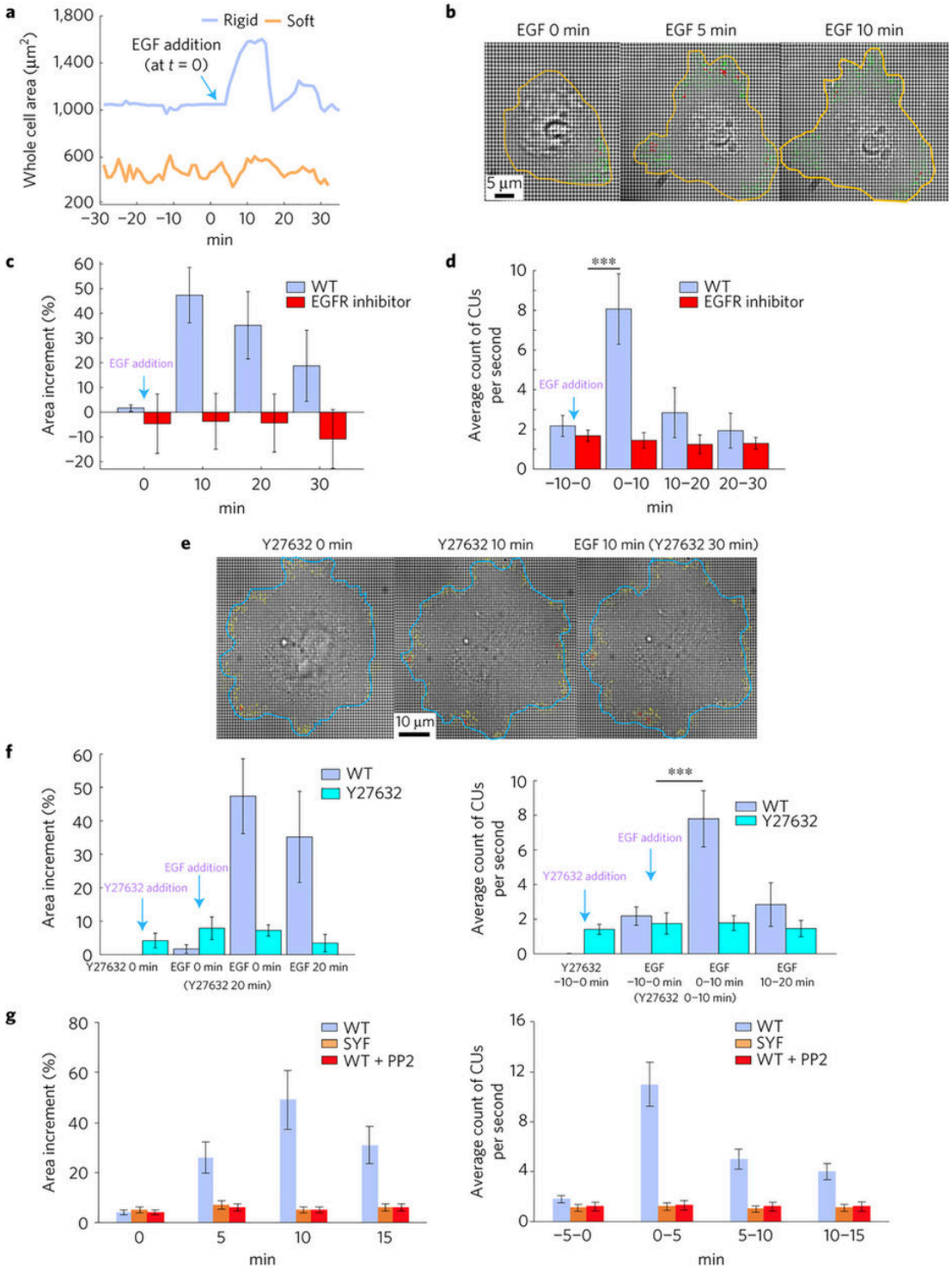

Figure 5 EGF activates local contraction activity. **a,** EGF (100 ng/ml) addition leads to cell

edge outward movement on rigid pillar substrate (blue) but not on soft (orange). Cells were plated on FN-coated pillar substrate for 6 h in media lacking serum prior to EGF administration. **b,** visualization of cell edge extension and increased CU number by EGF. The yellow line marks the cell edge at each mentioned time point after addition of EGF. The green arrows represent the pillar displacement in the active area and red arrows mark CUs. **c** & **d,** Area and CUs number change upon EGF addition. Measurement were carried out in two conditions: with or without EGFR inhibitor pretreatment for 20 min prior to EGF addition. **c**, percentage of increasing area of whole cell measured at 0, 10, 20, and 30 min relative to baseline area (-10 min**). d**, average of CUs number per 10 min before and after addition of EGF. **e**, Visualization of cell area over time upon ROCK inhibition and EGF treatment. After 6 h plating on stiff pillar substrate, cells were treated with 10 μM Y-27632 for 20 min followed by EGF stimulation. Blue line marks the cell edge at each mentioned time point after addition of EGF. The yellow arrows represent pillar displacement in the active area and red arrows mark CUs. **f,** left: percentage of increasing area measured at 0 min with Y-27632, 10 min with Y-27632, 10 min with EGF, and 20 min with EGF relative to baseline area (-10 min with Y-27632). right: average of CUs number per 10 min. **g,** Measurement similar to b was carried in three conditions: MEFs with or without PP2 inhibitor and SYF cells. left: percentage of increasing area of the whole cell measured at 0, 5, 10, and 15 min relative to baseline area (-5 min). right: average of CUs number per 5 min before and after addition of EGF. n>10 for each condition. n>5 independent experiments. Error bars show standard error of the mean. ***p<0.001, student's t-test.

EGF activation of motility requires myosin contractility and SFK

Next, we tested if myosin-II activity was required for EGF activation. Myosin-II contractile activity was mediated by MRLC[28], which can be phosphorylated by rho-kinase[29] (ROCK). Adding Y-27632 (an inhibitor of myosin-II ROCK-mediated activity) blocked EGF-induced local contractility. Although Y-27632 addition caused a small increase in spread area (Fig. 5e,f), there was no increase in the number of CUs. Further, after treatment with Y-27632 for 20 minutes, EGF stimulation of motility and contractility was lost (Fig. 5f). Thus, inhibition of ROCK-dependent activation of myosin-II contractility blocked EGF stimulated local contractile activity and cell edge spreading.

To test for a role of SFKs in EGF stimulation, we stimulated MEFs in the presence of PP2 and found that there was no significant area or contractile unit increase post EGF addition (Fig. 5g). Similar results were observed with EGF stimulation of SYF cells (Fig. 5g). Thus, EGF activation of spreading and contractility was downstream of SFK activity.

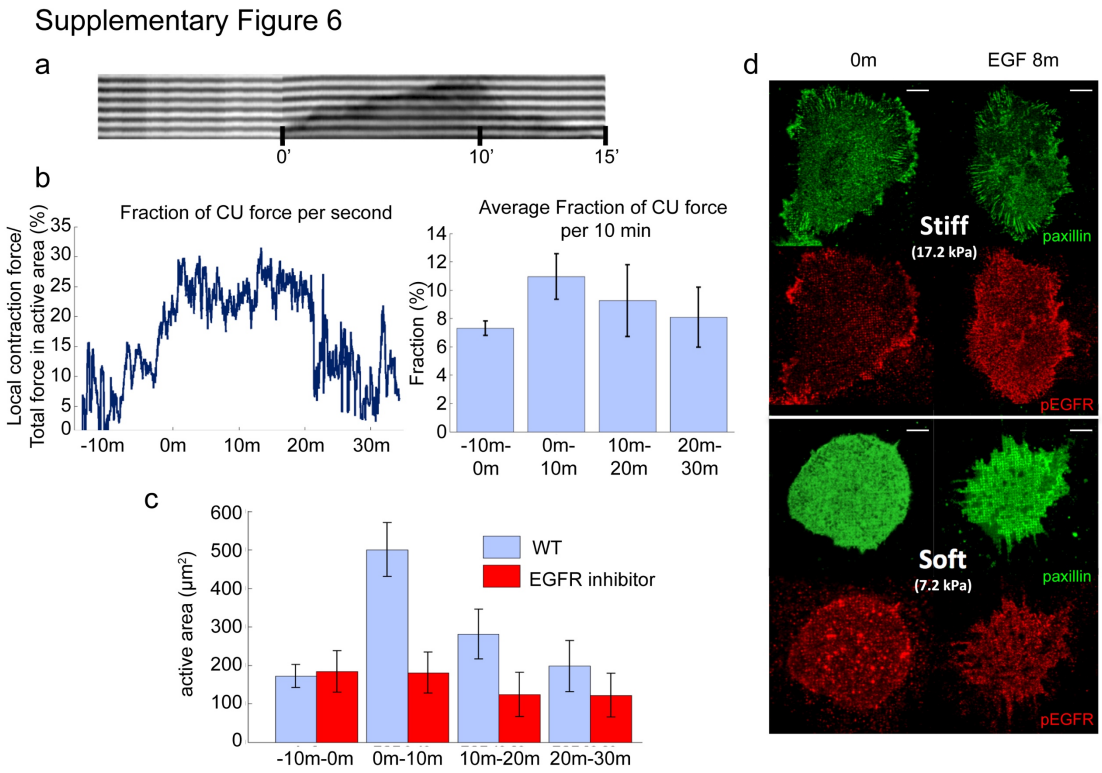

Supplementary Figure 6 EGF stimulation of cell edge and CU activity. **a,** Kymograph of cell edge after EGF addition at t=0 minutes. **b,** Plot of fraction of contractile unit force in total force exerted by the active area of a cell upon EGF addition. **c,** Active area of the cell with or without EGFR inhibitor when stimulated by EGF. **d,** Staining for paxillin and phosphorylated EGFR on rigid and soft substrates before (0 min) and after (8 min) addition of EGF. Scale bar is 10 □m. Error bars show standard error of the mean.

On soft surfaces EGF has no effect on rigidity sensing or motility

Since EGFR activity was not important for spreading and myosin contractility on soft surfaces, we wondered if EGF addition activated rigidity sensing on soft surfaces. After 6 hours on soft surfaces, cells changed spread area and morphology almost cyclically over periods of 30-45 minutes. When EGF was added to cells on soft pillar substrates, there was

no stimulation of spreading or CU activity. The cell area oscillations appeared unaltered following EGF addition (Fig. 5a). Further, EGF stimulation did not alter paxillin immunostaining on these substrates. Although EGF addition caused a significant increase in pEGFR in cells on soft surfaces, most pEGFR was not associated with adhesion complexes, contrary to cells on stiff pillars (Supplementary Fig. 4g and Supplementary Fig. 6d). These data are in line with previous results showing that reducing substrate rigidity desensitizes cells to EGF[30].

Discussion

Our results show that the EGFR and HER2 tyrosine kinases have a previously overlooked yet critical role in rigidity sensing. We find that rigidity sensing is dependent on EGFR activity. Surprisingly, EGFR activity has a significantly reduced role on soft surfaces and there is much less CU activity. This is partly explained by the fact that pEGFR localizes to integrin adhesions a lot more on rigid than on soft substrates. However, EGFR is only transiently associated with adhesions during their development, and once they are mature, their association with pEGFR is weak.

In this study, we show that EGFR and HER2 play a key role in rigidity sensing and directly affect CU formation. We find that during cell spreading, the formation of CUs is dramatically inhibited by blocking EGFR activity with the consequence that cell spread area is substantially decreased. The inhibition of SFK activity has a similar effect on CU activity and on spread area, which is consistent with earlier reports that Src kinase is responsible for non-ligand dependent activation of EGFR[1,2]. Furthermore, SFK mediated tyrosine phosphorylation can also activate overexpressed HER2 to substitute for EGFR in this pathway and enable rigidity sensing by the cell.

There is an extensive literature on EGFR because it has a major role in many cancers and growth abnormalities[3–5]. Our findings indicate that the non-ligand dependent activation of EGFR affects CU activity which we previously showed was important for rigidity sensing[6,7]. A simple hypothesis to explain the results is that EGFR is a critical part of a positive feedback system that is activated by rigid matrices. Since only a few studies of EGFR have been done on soft surfaces[8], the lack of EGFR involvement in cell function on

soft surfaces has not been well characterized. However, elements of the process can be understood.

Ligand-independent activation of EGFR is linked to Src activation of EGFR but only on rigid surfaces[9]. Our studies are consistent with SFK activation of EGFR that is dependent upon rigidity sensing and indicates that the recruitment of pEGFR to rigid adhesion sites depends upon SFK. Not only do the antibodies to the Src phosphorylation site on EGFR localize better to the adhesions than does the antibody to the autophosphorylation site, but also the inhibition of SFK has the same effect on spreading and CU activity as does the inhibition of EGFR kinase.

Our findings also highlight the transient nature of the EGFR effects. It is known that addition of EGF results in a transient (~1-3 minutes) activation of the EGFR that causes endocytosis and transport to the nucleus[10]. This addition of EGF to spread cells causes a dramatic increase in CU activity concomitant with the commonly observed rapid spreading. This effect of EGF is dependent upon myosin contractility and substrate rigidity, implying that there may be a positive feedback cycle for EGFR recruitment and activation of CU formation. The CUs are also dynamic since the contraction-relaxation cycle lasts only a minute[11]; and in stably spread cells, the level of CU activity is both very low and intermittent. However, on stiff surfaces, the CU activity causes the stabilization of adhesions and growth for many fibroblasts. If EGFR is an integral part of the system that causes CU assembly at adhesion sites, then it could also only transiently interact with the adhesions. Indeed, we find that the ratio of pEGFR to paxillin decreases upon adhesion maturation.

Furthermore, we show that the recruitment of pEGFR to adhesion sites depends upon SFK. Using mutants of the Src dependent phosphorylation sites we find that this pathway has a major role in the ligand-independent cellular rigidity sensing mechanism. We know that SFKs are activated in very early integrin adhesions and mere binding of soluble ligand to integrins leads to activation of SFKs even in the absence of force[24]. Further, Src phosphorylation is not affected in the absence of talin, a force bearing component of adhesions. Therefore, it makes sense that rigidity sensing will occur after SFKs are recruited and activated. We postulate that force is unfolding a protein such as talin in the adhesion clusters, which then binds EGFR and holds it for phosphorylation. Active EGFR could then further activate local myosin contraction through the known pathways downstream of EGFR involving PLC-dependent activation of PKC[15]. This positive feedback system could then cause further spreading and further SFK-dependent EGFR activation. Soft surfaces have short-lived adhesions that generate only weak forces, and thus they possibly would not recruit EGFR. Further, such a positive feedback scheme could explain the effect of EGF on formation of new CUs on rigid but not on soft surfaces or after inhibition of myosin contraction. Thus, we suggest that cell spreading and adhesion development involves EGFR in the formation but not in the maintenance of adhesions. All the evidence indicates that EGFR has a critical role in rigidity sensing that is dependent upon substrate rigidity and mechanical force. Although EGFR may have other roles that do not depend upon rigidity, it is clear both in the absence and presence of EGF that EGFR activity dramatically increases rigidity sensing on rigid surfaces and activates cell growth.

Materials and Methods

Procedure for Contractile unit (CU) Quantification

For measurement of CUs, pillar movements were analysed for pillars within about 4 micrometers of the edge. To allow for measurement of absolute displacement of the pillars, we followed pillars that were not initially in contact with the cell, but were beneath it after cell spreading. Data files with the position coordinates of cellular pillars and reference pillars were obtained from ImageJ Nano tracking plugin as described in the section 'Tracking pillar movements'. These data were then imported to a Matlab program to automatically generate force vector maps for the detected CUs and output the number of CUs per frame. Threshold parameters were set by users to identify CUs, including the time threshold (e.g. 20 s for MEFs), displacement threshold (>20 nm for 20 s) and space threshold (i.e. distance between neighbouring pillars). Therefore, CUs were identified on freshly contacted pillars with a detection criterion requiring that two or more neighboring pillars were pulled toward each other by more than 20 nm and for more than 20 seconds.

To verify the method, we visually counted the number of CUs then compared those results to the results generated by the program: miscounted CUs arose in cases when a pair of pillars that pointed perpendicular to each other were recognized as CUs (Supplementary Fig. 1a). The overall success rate of the automatic detection algorithm was 97.47±0.75% compared to the manual analysis.

Tracking pillar movements

Time-lapse imaging of pillars was performed with bright-field microscopy using an ORCA-Flash2.8 CMOS camera (Hamamatsu) attached to an inverted microscope

(Olympus IX-81), controlled by Micromanager software[31]. Images were recorded at 1 Hz using a 60x 1.4 NA, oil immersion objective (yielding a pixel size of 36 nm/pixel).

Videos were processed with ImageJ (National Institutes of Health) using the Nano Tracking plugin to track the position of pillars as explained previously[5,6]. The Nano Tracking plugin was based on a robust cross-correlation algorithm (resistant to particle shape variation) to track the position of pillars, and programmed to enable users to track all pillars in the appropriate areas automatically. To account for stage drift and illumination fluctuation, we analysed the movements of a set of reference pillars outside the cell, and subtracted their averaged movements from the movements of the pillars of interest. A low-pass filter (5 frame median filter) was used to smooth the stabilized movie before analysis for CUs.

Long-term CU measurement experiments

To reduce photo-damage to the cells during the long-term imaging, we tracked pillar movements intermittently for periods of 5-10 minutes every 30 or 60 minutes. When cells were observed with this protocol, there was no discernable photo-damage and this was validated by observing cells in the same dish at later times that had not previously been monitored. Thus, the method enabled us to monitor the number of CUs per cell for extended time periods. Cells were kept in a 37 °C, 5% CO_2 chamber on an inverted microscope, and a >600nm filter was to reduce photo-damage during imaging.

Continuous imaging over extended periods, i.e., imaging at 1 Hz continuously for many hours, led in many cases to a halt in cell spreading and later to blebbing and apoptosis. With the typical protocol that we used (periodic tracking of the pillar movements for periods of 5-10 minutes every half hour) we did not detect these effects. Further, cells that

were imaged in this way for >6 hours appeared very similar to other cells in the dish that were not illuminated during this period.

Pillar fabrication

Molds for making PDMS pillars were fabricated using electron beam lithography in hard Poly (methyl methacrylate) (PMMA) substrates. PMMA was first spun-coated onto a silicon substrate and then hard-baked on a hot plate for 10 hours. An electron beam lithography tool (NanoBeam nB5) was then used to pattern holes in the PMMA. The depth of holes was determined by the thickness of the PMMA. PDMS (mixed at 10:1 with its curing agent, Sylgard 184; Dow Corning) was then poured onto the PMMA moulds, cured at 70 °C for 12 h to reach a Young modulus of 2 ± 0.1 MPa, and demolded while immersed in 99.5 % isopropanol. All pillars had diameter D = 500 nm with 1000nm pitch. The top surfaces of the pillars were flat, with a height variation of only ~10% of pillar diameter. Pillar bending stiffness, k, was calculated by Euler–Bernoulli beam theory:

$$k = \frac{3}{64}\pi E \frac{D^4}{L^3}$$

where D and L are the diameter and length of the pillar, respectively, and E is the Young's modulus of the material (PDMS). k was further multiplied by a correction factor to take into account substrate warping at the base of the pillars[32]. In this paper, two different heights of pillars were fabricated for a stiff surface with effective modulus of 17.2 kPa (L1300 nm, effective stiffness=6 nN/μm) and a soft surface with effective modulus of 7.2 kPa (L1800, effective stiffness=2.5 nN/μm). The effective stiffness was calculated in accordance to the equation:

$$E\ (effective) = \frac{9}{4}\frac{k}{\pi A}$$

Where A is the typical length of adhesions forming on pillars[33].

The surfaces of the PDMS pillar substrates were coated with 10 μg/ml fibronectin for at least 1 hour prior to seeding cells. Scanning electron microscopy of fixed samples revealed that cell membranes only contacted the upper surface of the pillars and did not extend between pillars.

Flat substrate fabrication and preparation

For the 5.5 kPa substrate PDMS (1:1 Sylgard 527 part A:part B::1:1) was spread on glass bottom dishes and then incubated at 70 °C for 12 h. To achieve 50 kPa we mixed the Sylgard 527 mixture with Sylgard 184 mixture in accordance to the previously developed methods[34] and then incubated at 70 °C for 12 h. The surfaces of the PDMS gels were coated with 10 μg/ml fibronectin for at least 1 hour prior to seeding cells. Rigidity of the PDMS surfaces was measured by atomic force microscopy (AFM) indentation.

Cell Culture and Reagents

Mouse embryonic fibroblasts (MEFs) cells were generated by J. Sap's laboratory[35]. The cells were cultured at 37° C in a 5% CO_2 incubator in Dulbecco's Modified Eagle Medium (DMEM) supplemented with 10% fetal bovine serum (FBS), 100 IU/ml Penicillin-Streptomycin, and 2 μM L-Glutamine. The cells were tested for mycoplasma contamination and found negative. In all experiments, cells were serum-starved in growth medium lacking FBS. Imaging experiments were conducted using starvation medium without phenol red. Growth factors (all from Life Technologies) were diluted into 0.5 ml medium before adding to the specimen. The specific hormones used were mouse

recombinant EGF (100 ng/ml) and mouse recombinant TGFβ_1 (10 ng/ml). Pharmacological inhibitors and antibodies were as follows: Y-27632 (20μM, Calbiochem, Gibbstown, NJ), gefitinib (10 nM, Santa Cruz), PP2 (200 nM, abcam), pEGFR Tyr1173 (Santa Cruz, sc-12351), pEGFR Y1092 (abcam, equivalent to Y1068, EP774Y), paxillin (abcam, ab3127, 5H11, ab32084, BD Biosciences, 612405), pEGFR Y845 (abcam, ab5636), EGFR1 (abcam, ab30).

Several shRNA for EGFR were bought from Sigma Aldrich and tested. The knockdown results shown are with the shRNA TRCN0000055220 having the sequence "CCGGCCAAGCCAAATGGCATATTTACTCGAGTAAATATGCCATTTGGCTTGG TTTTTG". MEFs were transfected with Lipofectamine LTX using 4μg plasmid on Day 0 and then selected for transfection using Puromycin till all control cells died (Day 4 in our case). Then the selected transfected cells were used in the spreading experiment protocol.

Myosin IIA transfected Cos7 cells (Cos7-IIA) were selected using fluorescence activated cell sorting (FACs) and cultured in Dulbecco's modified Eagle's medium (DMEM) high glucose supplemented with 10% fetal bovine serum (FBS), 1 mM sodium pyruvate (Invitrogen) and 250 μg/ml selective antibiotics (G418) at 5% CO_2 at 37 C.

EGFR-GFP (plasmid #32751), EGFR-Y1045F-GFP (plasmid #40267), HER2-YFP (plasmid #66948) plasmids were purchased from Addgene. The EGFR-Y845F and HER2-Y879F (Rat sequence, equal to Human sequence Y877) mutants were generated using primers 5'AGAGAAAGAATTCCATGCAGAAGGAGG3' (EGFR), 5'TCCGCACCCAGCAGTTG-3' (EGFR), 5'TGAGACAGAGTTCCATGCAGATG-3' (HER2), 5'-TCAATGTCCAGCAGCCGA3' (HER2), following the protocol provided in Q5 Site-Directed Mutagenesis Kit (NEB). Cells were seeded into a 6-well plate with 60-

70% confluence at day 0 and transfected with 25 μM of EGFR siRNA (Qiagen, pre-mix EGFR siRNA, catalogue no. SI00300104) using lipofectamine RNAiMAX (Invitrogen) on day 1. Control cells were transfected with scrambled control siRNA. Transfection of rescue plasmids were performed by on day 3 using lipofactamine 2000 (Invitrogen) following the manufacturer's instructions.

Quantification of peripheral localization of pEGFR

In order to assess the population of cells showing peripheral localization of pEGFR we used a relative intensity ratio metric calculated on images of cells stained for various pEGFR sites when spread on different rigidities. Cells were stained and then imaged using the exact same imaging conditions. Two areas - peripheral area (Area 1, up to 5 micrometers from the edge) near the cell edge and inner area (Area 2) - were marked on the image (Supplementary Fig. 3a). Then the Intensity ratio (I) was calculated as:

$$Intensity\ Ratio\ (I) = \frac{Mean\ Intensity\ Area\ 1}{Mean\ Intensity\ Area\ 2}$$

This ratio was a measure of relative localization of intensity near cell edge.

Statistical Analyses

Sample sizes were chosen to test whether the distributions of the populations were normal, and t-tests were performed where noted. In the case of pEGFR colocalization with paxillin, analyses were performed by calculating the Pearson's correlation coefficient between the two channels.

For long-term live cell tracking, the number of samples was ~10 in each case; however, we compared the results from the live cell movies to randomly chosen cells on the dish at specific time points (the latter n was >30), and the results were comparable.

Code Availability

MATLAB code used for identifying CUs is available upon request.

Data Availability

The data that support the findings of this study are available from the corresponding author upon reasonable request.

References

1. Wang, H. B., Dembo, M. & Wang, Y. L. Substrate flexibility regulates growth and apoptosis of normal but not transformed cells. *Am. J. Physiol. Cell Physiol.* **279,** C1345-1350 (2000).
2. Engler, A. J., Sen, S., Sweeney, H. L. & Discher, D. E. Matrix elasticity directs stem cell lineage specification. *Cell* **126,** 677–89 (2006).
3. Lo, C. M., Wang, H. B., Dembo, M. & Wang, Y. L. Cell movement is guided by the rigidity of the substrate. *Biophys J* **79,** 144–52 (2000).
4. Elosegui-Artola, A. *et al.* Rigidity sensing and adaptation through regulation of integrin types. *Nat. Mater.* **13,** 631–637 (2014).
5. Ghassemi, S. *et al.* Cells test substrate rigidity by local contractions on submicrometer pillars. *Proc Natl Acad Sci U A* **109,** 5328–33 (2012).

6. Wolfenson, H. *et al.* Tropomyosin controls sarcomere-like contractions for rigidity sensing and suppressing growth on soft matrices. *Nat Cell Biol* **18,** 33–42 (2016).
7. Meacci, G. *et al.* α-Actinin links extracellular matrix rigidity-sensing contractile units with periodic cell-edge retractions. *Mol. Biol. Cell* **27,** 3471–3479 (2016).
8. Yang, B. *et al.* Mechanosensing Controlled Directly by Tyrosine Kinases. *Nano Lett.* **16,** 5951–5961 (2016).
9. Sato, K.-I. Cellular functions regulated by phosphorylation of EGFR on Tyr845. *Int. J. Mol. Sci.* **14,** 10761–10790 (2013).
10. Bill, H. M. *et al.* Epidermal growth factor receptor-dependent regulation of integrin-mediated signaling and cell cycle entry in epithelial cells. *Mol. Cell. Biol.* **24,** 8586–8599 (2004).
11. Huveneers, S. & Danen, E. H. J. Adhesion signaling – crosstalk between integrins, Src and Rho. *J. Cell Sci.* **122,** 1059–1069 (2009).
12. Eberwein, P. *et al.* Modulation of focal adhesion constituents and their down-stream events by EGF: On the cross-talk of integrins and growth factor receptors. *Biochim. Biophys. Acta BBA - Mol. Cell Res.* **1853,** 2183–2198 (2015).
13. Schneider, I. C., Hays, C. K. & Waterman, C. M. Epidermal Growth Factor–induced Contraction Regulates Paxillin Phosphorylation to Temporally Separate Traction Generation from De-adhesion. *Mol. Biol. Cell* **20,** 3155–3167 (2009).
14. Moasser, M. M. The oncogene HER2: its signaling and transforming functions and its role in human cancer pathogenesis. *Oncogene* **26,** 6469–6487 (2007).

15. Iwabu, A., Smith, K., Allen, F. D., Lauffenburger, D. A. & Wells, A. Epidermal growth factor induces fibroblast contractility and motility via a protein kinase C delta-dependent pathway. *J. Biol. Chem.* **279,** 14551–14560 (2004).
16. Geiger, B., Bershadsky, A., Pankov, R. & Yamada, K. M. Transmembrane crosstalk between the extracellular matrix and the cytoskeleton. *Nat Rev Mol Cell Biol* **2,** 793–805 (2001).
17. Wolfenson, H., Lavelin, I. & Geiger, B. Dynamic regulation of the structure and functions of integrin adhesions. *Dev Cell* **24,** 447–58 (2013).
18. Ménard, S., Tagliabue, E., Campiglio, M. & Pupa, S. M. Role of HER2 gene overexpression in breast carcinoma. *J. Cell. Physiol.* **182,** 150–162 (2000).
19. Giannone, G. *et al.* Periodic lamellipodial contractions correlate with rearward actin waves. *Cell* **116,** 431–43 (2004).
20. Cabodi, S. *et al.* Integrin regulation of epidermal growth factor (EGF) receptor and of EGF-dependent responses. *Biochem. Soc. Trans.* **32,** 438–442 (2004).
21. Yamada, K. M. & Even-Ram, S. Integrin regulation of growth factor receptors. *Nat. Cell Biol.* **4,** E75–E76 (2002).
22. Balanis, N. & Carlin, C. R. Mutual cross-talk between fibronectin integrins and the EGF receptor: Molecular basis and biological significance. *Cell. Logist.* **2,** 46–51 (2012).
23. Cai, Y. *et al.* Nonmuscle myosin IIA-dependent force inhibits cell spreading and drives F-actin flow. *Biophys J* **91,** 3907–20 (2006).
24. Seshacharyulu, P. *et al.* Targeting the EGFR signaling pathway in cancer therapy. *Expert Opin. Ther. Targets* **16,** 15–31 (2012).

25. Xu, K.-P., Yin, J. & Yu, F.-S. X. SRC-family tyrosine kinases in wound- and ligand-induced epidermal growth factor receptor activation in human corneal epithelial cells. *Invest. Ophthalmol. Vis. Sci.* **47,** 2832–2839 (2006).
26. Iskratsch, T. *et al.* FHOD1 Is Needed for Directed Forces and Adhesion Maturation during Cell Spreading and Migration. *Dev Cell* **27,** 545–59 (2013).
27. Lauffenburger, D. A. & Horwitz, A. F. Cell migration: a physically integrated molecular process. *Cell* **84,** 359–69 (1996).
28. Adelstein, R. S. & Anne Conti, M. Phosphorylation of platelet myosin increases actin-activated myosin ATPase activity. *Nature* **256,** 597–598 (1975).
29. Matsui, T. *et al.* Rho-associated kinase, a novel serine/threonine kinase, as a putative target for small GTP binding protein Rho. *EMBO J.* **15,** 2208–2216 (1996).
30. Kim, J.-H. & Asthagiri, A. R. Matrix stiffening sensitizes epithelial cells to EGF and enables the loss of contact inhibition of proliferation. *J Cell Sci* **124,** 1280–1287 (2011).

Discussion references

1. Andreev, J. *et al.* Src and Pyk2 mediate G-protein-coupled receptor activation of epidermal growth factor receptor (EGFR) but are not required for coupling to the mitogen-activated protein (MAP) kinase signaling cascade. *J. Biol. Chem.* **276,** 20130–20135 (2001).
2. Moro, L. *et al.* Integrin-induced epidermal growth factor (EGF) receptor activation requires c-Src and p130Cas and leads to phosphorylation of specific EGF receptor tyrosines. *J. Biol. Chem.* **277,** 9405–9414 (2002).

3. Normanno, N. *et al.* Epidermal growth factor receptor (EGFR) signaling in cancer. *Gene* **366,** 2–16 (2006).
4. Tang, X. *et al.* Epidermal growth factor receptor abnormalities in the pathogenesis and progression of lung adenocarcinomas. *Cancer Prev. Res. Phila. Pa* **1,** 192–200 (2008).
5. Brand, T. M., Iida, M., Li, C. & Wheeler, D. L. The nuclear epidermal growth factor receptor signaling network and its role in cancer. *Discov. Med.* **12,** 419–432 (2011).
6. Ghassemi, S. *et al.* Cells test substrate rigidity by local contractions on submicrometer pillars. *Proc Natl Acad Sci U A* **109,** 5328–33 (2012).
7. Wolfenson, H. *et al.* Tropomyosin controls sarcomere-like contractions for rigidity sensing and suppressing growth on soft matrices. *Nat Cell Biol* **18,** 33–42 (2016).
8. Kim, J.-H. & Asthagiri, A. R. Matrix stiffening sensitizes epithelial cells to EGF and enables the loss of contact inhibition of proliferation. *J Cell Sci* **124,** 1280–1287 (2011).
9. Wang, Y. *et al.* Pseudopodium-enriched atypical kinase 1 regulates the cytoskeleton and cancer progression [corrected]. *Proc Natl Acad Sci U A* **107,** 10920–5 (2010).
10. Xu, K.-P., Yin, J. & Yu, F.-S. X. SRC-family tyrosine kinases in wound- and ligand-induced epidermal growth factor receptor activation in human corneal epithelial cells. *Invest. Ophthalmol. Vis. Sci.* **47,** 2832–2839 (2006).
11. Iskratsch, T. *et al.* FHOD1 Is Needed for Directed Forces and Adhesion Maturation during Cell Spreading and Migration. *Dev Cell* **27,** 545–59 (2013).

References contd.

31. Stuurman, N., Edelstein, A. D., Amodaj, N., Hoover, K. H. & Vale, R. D. Computer Control of Microscopes using μManager. *Curr. Protoc. Mol. Biol. Ed. Frederick M Ausubel Al* **CHAPTER,** Unit14.20 (2010).
32. Schoen, I., Hu, W., Klotzsch, E. & Vogel, V. Probing Cellular Traction Forces by Micropillar Arrays: Contribution of Substrate Warping to Pillar Deflection. *Nano Lett.* **10,** 1823–1830 (2010).
33. Ghibaudo, M. *et al.* Traction forces and rigidity sensing regulate cell functions. *Soft Matter* **4,** 1836–1843 (2008).
34. Palchesko, R. N., Zhang, L., Sun, Y. & Feinberg, A. W. Development of polydimethylsiloxane substrates with tunable elastic modulus to study cell mechanobiology in muscle and nerve. *PLoS One* **7,** e51499 (2012).
35. Su, J., Muranjan, M. & Sap, J. Receptor protein tyrosine phosphatase alpha activates Src-family kinases and controls integrin-mediated responses in fibroblasts. *Curr Biol* **9,** 505–11 (1999).

Chapter 4

Explore the role of calpain cleavage of talin in adhesion development and rigidity sensing

Abstract

Cell growth depends upon formation of cell-matrix adhesions, but mechanisms detailing the transmission of signals across adhesions to control proliferation are lacking. Here, we find that the scaffold protein talin undergoes force-induced cleavage in early adhesions to produce the talin rod fragment that is needed for cell cycle progression. Expression of non-cleavable talin blocks cell growth, adhesion maturation, proper mechanosensing, and the related property of EGF activation of motility. Further, the expression of talin rod in the presence of non-cleavable full-length talin rescues cell growth and other functions. The cleavage of talin is found in early adhesions where there is also rapid turnover of talin that depends upon calpain and TRPM4 activity as well as the generation of force on talin. Thus, we suggest that an important function of talin is its control over cell cycle progression through its cleavage in early adhesions.

Introduction

Cells receive critical mechanical signals from integrin-mediated cell-matrix adhesions that control many cellular processes in wound healing, development, and cancer[1–3]. One of the most important cellular functions affected by such signals is cell growth, evidenced by the inability of non-transformed cells to proliferate on soft surfaces that do not support strong adhesion (soft-agar assays). Transmission and processing of mechanical signals rely upon the dynamic regulation of the adhesions, which is tightly coordinated with activation of intracellular signaling cascades. However, we don't understand the molecular mechanisms of mechanical signals that are transmitted through the adhesions to control growth.

Studies of the spreading of fibroblasts on fibronectin (FN)-coated surfaces have revealed many aspects of adhesion dynamics, including a role for talin in activation of integrins, which is an essential step for cell-substrate attachment[4,5]. Talin is one of the earliest molecules to arrive at nascent adhesion sites[6–8], and is involved in mechanosensing through the adhesions[9]. Talin is also a substrate for calpain mediated cleavage, and calpain activity is important during the dissolution of mature matrix adhesions[10,11]. Upon calpain inhibition, cells have large and more frequent adhesions. Furthermore, talin cleavage generates talin head and rod fragments that affect independent downstream cellular functions. Talin rod, for example, activates cell proliferation and cell cycle progression in the absence of full-length talin[12]. However, whether talin cleavage plays a role in transmitting mechanical signals during mechanosensing through early adhesions is unknown.

Here, we show that talin cleavage is a key cellular mechanism regulating proper adhesion formation, in the absence of which cells show inhibited growth and cell motility is not stimulated by EGF. Some of these effects could be rescued by the expression of free talin rod fragment, emphasizing the importance of talin cleavage in cell cycle progression. We also show that forces applied at the cell edge during mechanosensing of the matrix induce talin cleavage. Interestingly, non-cleavable talin also alters talin turnover kinetics in early adhesions, and causes integrin clustering to a much higher density than the talin head, rod, or full length molecule. Non-cleavable talin alters mechanosensing forces and normal behavior is restored by the expression of talin rod fragment but not talin head, emphasizing the specific role of the rod fragment even in the presence of the full-length molecule. This supports the idea that force-induced talin cleavage during mechanosensing is necessary for proper adhesion formation and the cleavage products are critical components of cellular functions.

Results

Lack of talin cleavage inhibits cellular proliferation and EGF stimulation of cell motility

Since control over proper adhesion formation affected cell proliferation[13,14] and talin cleavage was needed for normal adhesion behavior, we expressed a non-cleavable form of talin1 (NC-talin, L432G)[10] in talin1-/- cells and tested if NC-talin had an effect on cell proliferation (see Methods). In a mixed population of talin1-/- cells with and without either WT-talin-GFP or NC-talin-GFP expression, the talin1-/- cells grew faster than those with either talin1 form; however, over the course of 10 days, the WT-talin-GFP expressing cells grew whereas the NC-talin-GFP cells decreased in number (Fig. 1a).

To determine if talin cleavage effected other cell behaviors, we added epidermal growth factor (EGF) to stimulate spread cells – a treatment that was previously shown to activate

cell edge movement and adhesion formation[15,16]. After spreading WT- and NC-talin cells

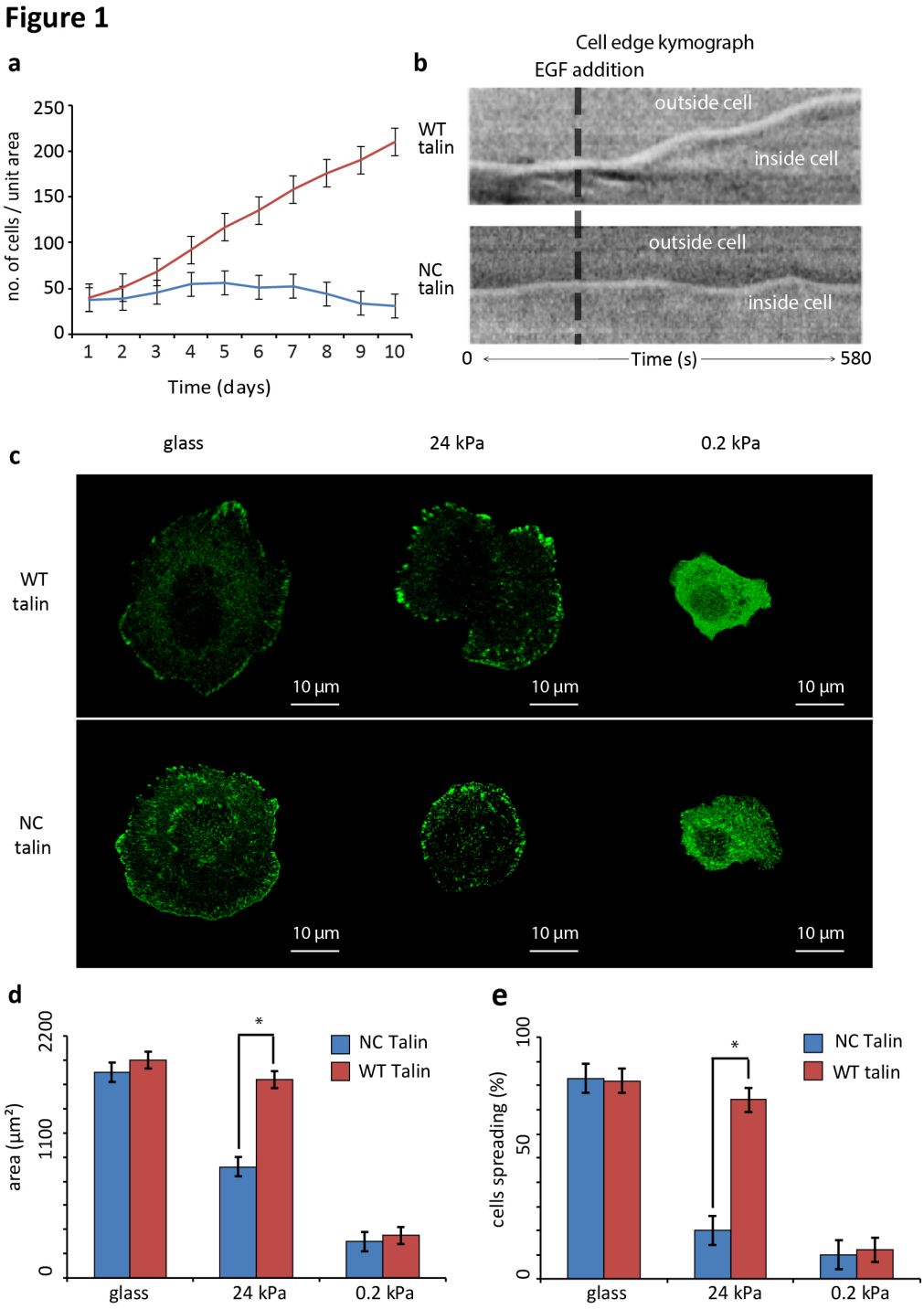

Fig. 1 Calpain-mediated talin cleavage affects cell growth and rigidity sensing. **a**, Cell growth curves showing transfected cells per unit area for individual experiments for WT-

or NC-talin cells cultured on glass in the presence of serum. **b**, Cell edge kymograph of a single WT- or NC- talin expressing cell. The dashed line indicates EGF addition. **c**, Talin 1-/- cells expressing WT- or NC-talin were allowed to spread for 25 minutes on FN-coated substrates: glass, 24 kPa gel, or 0.2 kPa gel. **d**, Average area of spreading cells as detailed in panel **c. e**, Percentage of cells spreading as detailed in panel. n>30 for panels **d** and **e.** The experiment was repeated 4 times.

on FN-coated glass for 6 hours, they were stimulated with 100 ng/ml EGF. Whereas WT-talin cells displayed increased protrusion-retraction cycles of the cell edge upon EGF addition, the edges of NC-talin cells remained largely inactive and kept collapsing after minor fluctuations (kymograph of cell edge over ~10 minutes in Fig. 1b). After EGF addition, there was a roughly 50 percent increase in whole cell area for WT-talin cells but NC-talin cells were unaffected (Supplementary Fig. 1a,b). This indicated that talin cleavage was required for motility activation by EGF. In a recent study, we showed that the EGF stimulation of cell motility was rigidity dependent and cells reacted much less to EGF on softer substrates[17]. Therefore, we hypothesized that NC-talin cells were underestimating substrate rigidity because of a faulty adhesion development mechanism.

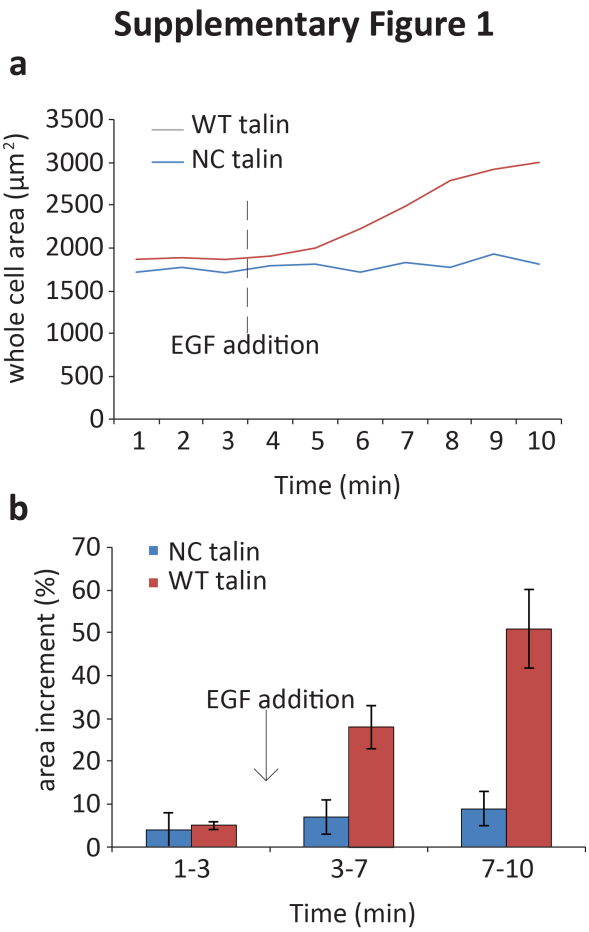

Supplementary Fig. 1 Talin cleavage is required for EGF stimulation of cells **a**, Whole cell area for a single cell (WT or NC-talin expressing cell) spreading on glass and stimulated by EGF. **b**, Percentage of increment in cell spreading area upon EGF addition when compared to that at 0 minutes as in **a**. n>10 for each type.

Talin cleavage at L432 is necessary for proper adhesion formation and accurate rigidity sensing

We next sought out to test if talin cleavage had a role in the early adhesion formation and rigidity sensing. Previous studies showed that early integrin adhesions played a significant role in sensing matrix rigidity[18–21], evident in effects on the level of cell spreading.

Therefore, we tested early cell spreading on FN-coated surfaces of different rigidities. When plated on FN-coated glass (an extremely stiff surface) for 30 minutes, NC-talin cells spread to a similar area as WT-talin cells (Fig. 1c,d), although they had larger adhesions, as reported earlier[11]. A more pronounced difference between WT- and NC-talin cells appeared when they were plated on FN-coated Polydimethylsiloxane (PDMS) gels or pillars with an effective substrate rigidity of 24 kPa (see Methods). Whereas WT-talin cells spread to ~1500 μm^2 area after 30 minutes, NC-talin cells spread to a ~2-fold lower area (Fig. 1c,d, Supplementary Fig. 2a,b). Notably, over 80% of NC-talin cells failed to form an active edge (Supplementary Fig. 2c) and did not spread beyond their initial attachments to the 24 kPa substrate (Fig. 1d); however, they typically remained adherent to the substrate and could not be easily removed by e.g. shaking of the substrate. In the other extreme scenario, WT-talin cells plated on ultra-soft surfaces (0.2 kPa) did not spread and were not distinguishable from the NC-talin cells after 30 minutes of spreading (Fig. 1c,d,e). Similar results were obtained when we repeated the spreading experiments after talin2 knockdown in talin1-/- cells (data not shown), indicating that talin2 did not have a role in these phenomena. Thus, NC-talin was not able to support proper cell spreading on intermediate rigidity surfaces and cells behaved as if they were on much softer substrates.

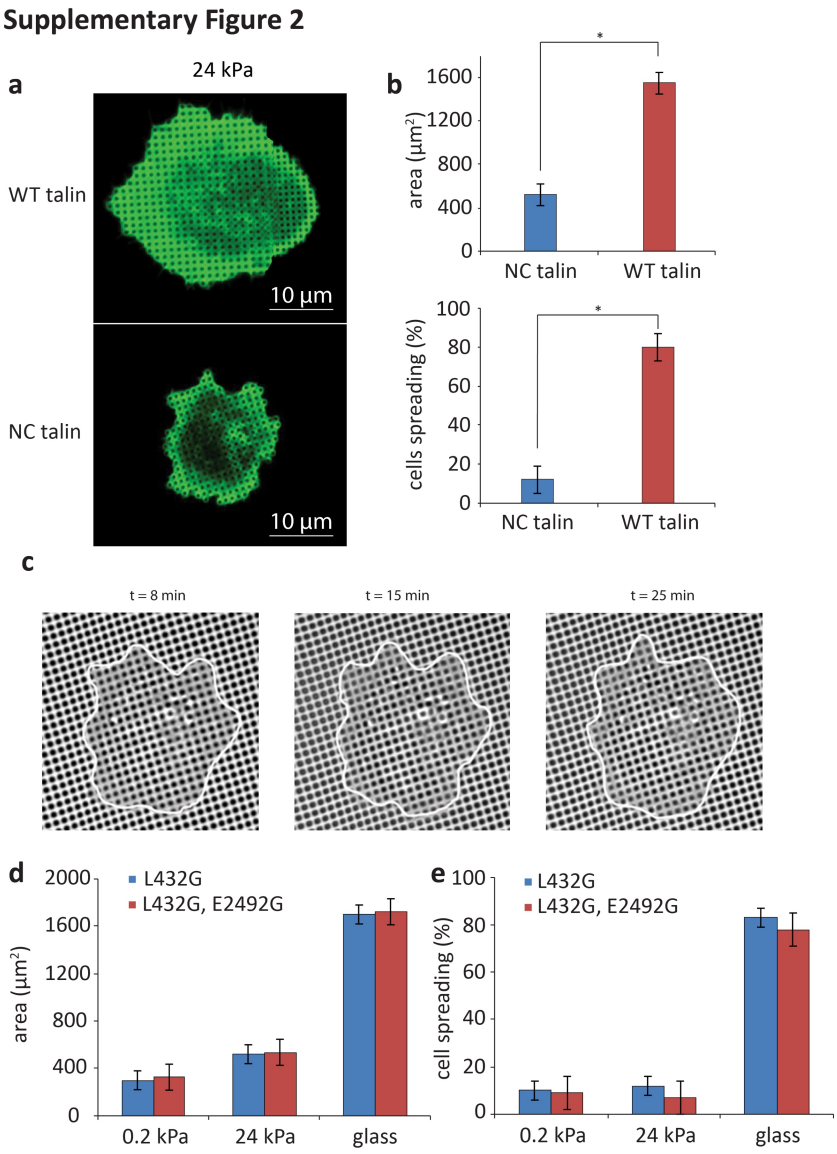

Fig. S2 Talin cleavage is important to sustain spreading. **a**, WT or NC-talin expressing cells on 24kPa pillar array after 25 minutes. **b**, Average cell spreading area and average percentage of cells spreading for cells as in panel **a**. **c**, NC-talin expressing cell on 24 kPa pillar array at 8, 15 and 25 minute after seeding. n>30 for panels **b** and **c**. Talin cleavage at primary cleavage site L432 affects early cell spreading. **d**, Average whole cell area of cells expressing either single site talin mutant (L432G) or double site talin mutant (L432G, E2492G) when spread on substrates of different rigidities (0.2 kPa, 24 kPa, glass). **e**, Percentage of spreading cells on different rigidity substrates. n>20 for each type in **d** and **e**.

Talin has another calpain cleavage site near its C-terminus that was significantly less susceptible to cleavage[11]. To test for a possible role of this other site, we expressed a double mutant of talin, where both calpain cleavage sites were rendered non-cleavable (L432G, E2492G) in talin1-/- cells, and performed the same cell spreading experiments. The results were not distinguishable from those observed with L432G (Supplementary Fig. 2d,e). Further, cells expressing talin with a single mutation of the second cleavage site (E2492G) showed normal cellular area (data not shown) on all substrates. This indicated that calpain cleavage at L432 was critical for accurate rigidity sensing, with little or no contribution from the E2492 cleavage site. Therefore, we used the L432G talin mutant for all subsequent experiments.

Ratio of talin rod to head confirms talin cleavage at adhesion sites

Earlier studies linked calpain-mediated proteolysis of talin to turnover of mature focal adhesions[10,11], but it was not known whether talin cleavage occurred during formation of adhesions. Although our results indicated that cleavage occurred during adhesion formation, we wanted to quantify the process. To establish talin cleavage at early adhesion sites, we expressed GFP-talin1-mCherry or GFP-NC-talin1-mCherry in talin1-/- cells. Since the calpain cleavage site was in the linker between talin head and rod (Fig. 2a), we postulated that a difference in the number of GFP and mCherry fluorophores would validate talin cleavage at early adhesion sites near the cell edge. In the past we found that cells formed early adhesions at their edges on individual pillar tops and exerted cytoskeletal forces on the pillars[19–21]. With time, those early adhesions grew and formed longer mature adhesions (Supplementary Fig. 3a). This discrete adhesion development, on separate pillars, was ideal for counting adhesion molecules, potentially under force. To establish the

role of talin cleavage in early adhesions, we counted the relative numbers of GFP and mCherry molecules at each pillar top under a spreading cell edge where new adhesions formed. To that end, we plated the cells on 24 kPa PDMS pillars coated with FN and allowed them to spread for 20 minutes before fixing them with formaldehyde. After focusing on the pillar tops under a cell edge with characteristic spreading morphology (Fig. 2b), we continuously recorded the fluorescence intensities of the GFP and mCherry fluorophores over time with high intensity illumination until they were completely bleached.

Figure 2

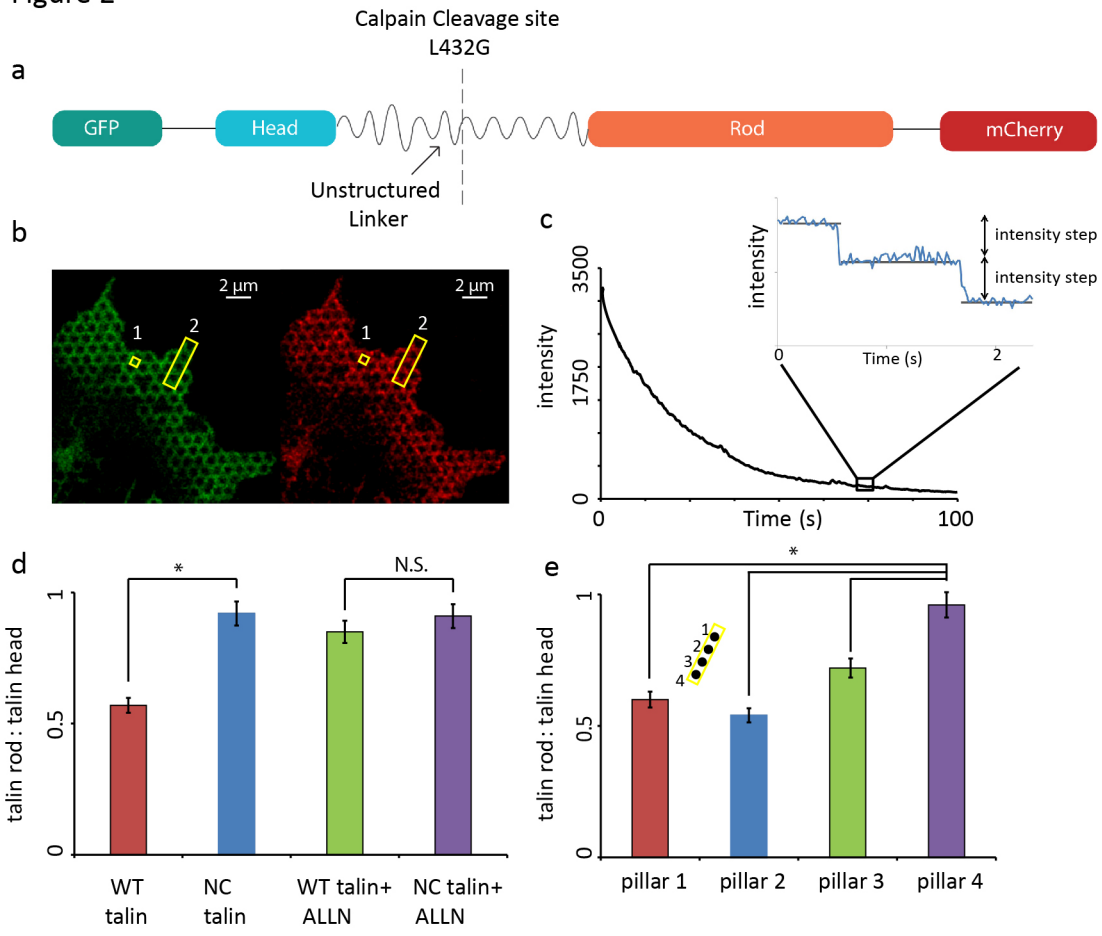

Fig. 2 Molecule counting of double-tagged talin reveals its cleavage. **a**, Talin schematic

showing talin head, talin rod, the position of GFP, mCherry fluorophores, and site of mutation (L432G) in the linker region which renders talin 1 non-cleavable by calpain. Not to scale. **b**, Cells expressing the double-tagged talin molecule. Boxes 1 and 2 are the ones used for analysis of intensity in **c**, **d,** or **e**. **c,** Bleaching curve for Box 1 in panel **b**, for the GFP channel. Zoom-in shows single steps in intensity during bleaching, which account for single GFP molecules. Similar steps (with different step size) were found for mCherry. These steps were used for counting the number of GFP and mCherry molecules at the cell edge in unbleached regions by dividing the initial intensity by the average intensity of the bleaching steps. **d**, Plot of the ratio of the number of GFP and mCherry molecules at the cell edge. Ratio was also plotted when cells were spread in the presence of Calpain inhibitor (ALLN). This ratio is a measure of talin rod: talin head. **e**, Distribution of talin rod: talin head ratio at different distances from cell edge. Pillar 1 is closest to cell edge and pillar 4 closest to nucleus (Box 2 in **b**).

Near the end of the bleaching process, we identified single fluorophore bleaching events for both GFP and mCherry as single steps in the fluorescence intensity curves (Fig. 2c). Using many such steps, we established the average fluorescence intensity levels for single fluorophores of GFP and mCherry (see Supplementary Fig. 3b,c). The single fluorophore (1X) and double fluorophore peaks (2X) were clearly visible in the histogram. Once the intensity step size for a single fluorophore was established, we determined the original number of GFP and mCherry molecules at adhesion sites (Box 1, Fig. 2b) and calculated their ratio. Whereas the mCherry/GFP ratio of NC-talin was close to 1 (0.90±0.05, n=43, 6 cells), it was 0.57±0.03 for WT-talin (n=54, 8 cells) (Fig. 2d). When we spread WT-talin

cells in the presence of a calpain inhibitor (ALLN), the ratio near the cell edge increased

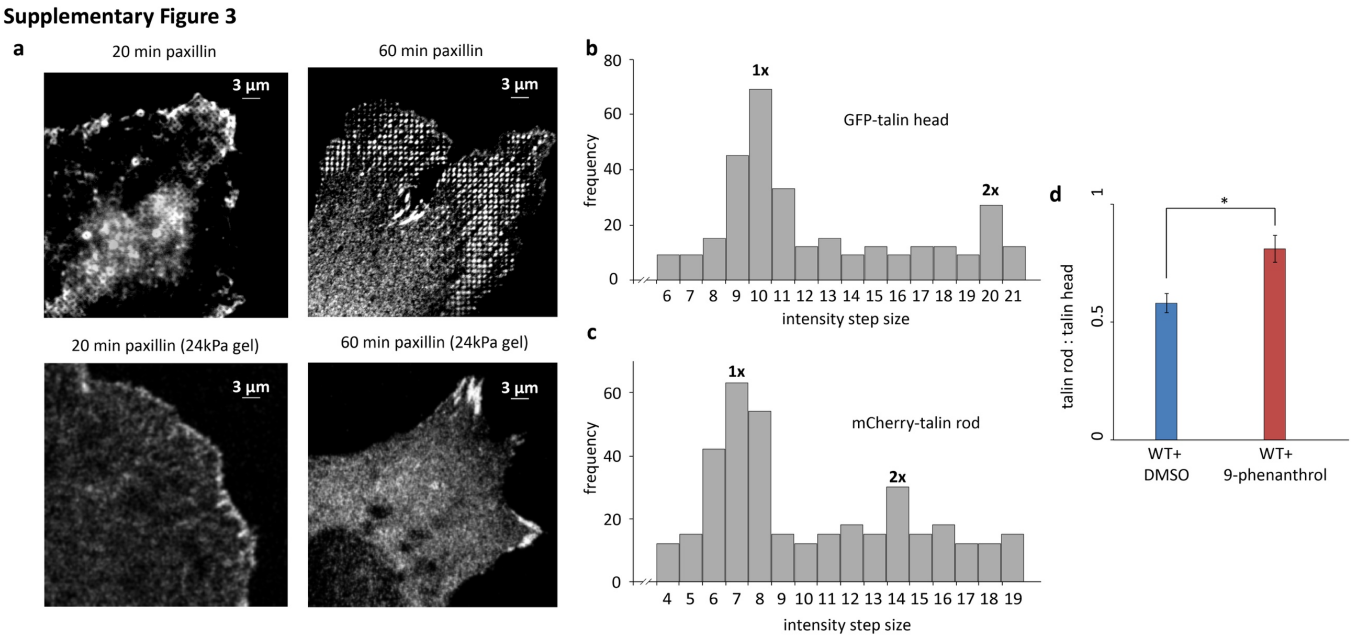

Fig. S3 Adhesions grow on both flat and pillar substrates and Calcium channel inhibition blocks talin cleavage. **a**, Cells spread on 24 kPa pillar array or 24 kPa PDMS showing Paxillin distribution at 20 and 60 minutes. **b**, Histograms of intensity steps observed at several single pillar tops (box 1 Fig. 3b) for GFP-talin head and **c**, mCherry-talin rod. The peaks at 1x step size and 2x step were clearly visible. **d**, Ratio of talin rod to talin head with TRPM4 channel inhibitor 9-phenanthrol or DMSO. 28 pillars, 8 cells.

to similar values as in the NC-talin case (0.83±0.05, n= 58, 8 cells). Addition of the same inhibitor to NC-talin expressing cells had no significant effect (Fig. 2d). Further, since calpain activity was dependent on Ca^{2+}, and given that the TRPM4 channel localized to the leading edges of fibroblasts[22], we tested if the TRPM4 inhibitor (9-phenanthrol) had an effect. In the presence of the inhibitor, the mCherry/GFP ratio was also close to 1 (Supplementary Fig. 3d). Cell spreading was also altered, as was adhesion formation,

basically recapitulating the cell behavior with NC-talin. Taken together, these results confirmed that fluorophore counting could be used as a measure of talin cleavage at early adhesion sites and that cleavage was blocked by inhibiting calpain.

The cleavage of talin at early adhesion sites along with the significant rigidity-dependent effects in the presence of NC-talin (Fig. 1) indicated that talin cleavage was critical for the process of rigidity sensing. Our previous studies showed that rigidity sensing occurred in a region ~2-3 μm from the cell edge, but not further back from the edge[19–21]. We therefore analyzed the mCherry/GFP ratio of WT-talin as a function of distance from the cell edge (Box 2, Fig. 2b). This analysis showed that the mCherry/GFP ratio was nearly 1 on pillars closer to the nucleus, but decreased when approaching the cell edge (Fig. 2e). This indicated a correlation between cellular forces at early adhesion sites and talin proteolysis.

Rapid talin cleavage occurs during early traction force development and decreases after peak forces

To further test the idea that talin cleavage was linked to cellular forces, we seeded cells expressing GFP-talin1-mCherry on FN coated 24 kPa pillars, and performed live cell imaging in 3 channels (green, red, and brightfield) as shown in Fig. 3a (Zoom-in from Supplementary Fig. 4a). To determine the dynamic fluorophore counts of talin GFP-head and mCherry-rod (Fig. 3b), we converted the mCherry and GFP intensity into the number of molecules using the factor from the counting experiments (Fig. 2), since the imaging conditions were identical.

Figure 3

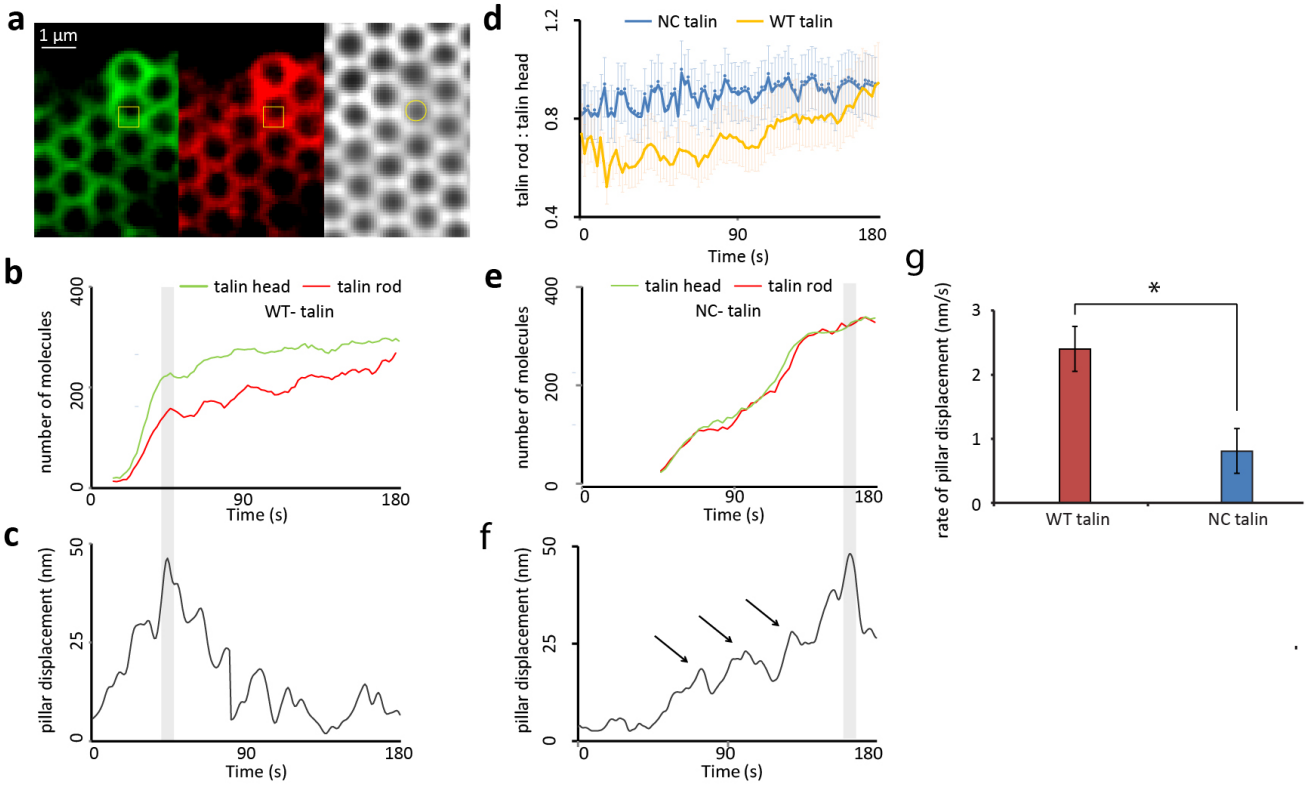

Fig. 3 Talin cleavage is a rapid, force-dependent process and substrate deformation cannot be sustained in the absence of it. **a**, Experimental setup for live cell imaging of cells expressing double tagged WT- or NC-talin along with simultaneous pillar displacement tracking. The magnitude of pillar displacement is directly related to traction force. One adhesion site corresponding to a single pillar is marked in yellow box. The tracked pillar is marked by a yellow circle. **b**, Observed intensity was converted to number of molecules using conversion factors determined in Fig. 2 and plotted for both talin head and talin rod for a cell expressing WT-talin. **c**, simultaneous pillar displacement for the same pillar in panel **b** is plotted. **d**, Ratio of talin rod to head as a function of time (t=0 is first contact of membrane with pillar top) for WT- and NC-talin. **e**, Number of talin head and rod

molecules for a single adhesion site as in the yellow box in panel **a** for a cell expressing NC-talin. **f**, Simultaneous pillar displacement for the same pillar as in panel **e**. Arrows indicate breaks in pillar displacement. **g**, Rate of pillar displacement for WT or NC-talin cells. n>40 (pillars) in 12 cells.

Brightfield images enabled the simultaneous measurement of the displacement of pillars (Fig. 3c). Initially, there was a roughly linear increase in the intensity of talin head (GFP) and talin rod (mCherry) (from time=0 until the grey band in Figure 3b). In parallel, the displacement of the same pillars increased steadily (Fig. 3c, Supplementary Fig. 4b). With WT-talin, the mCherry/GFP ratio showed an initial drop, followed by fluctuations at about 0.6 (Fig. 3d). When the pillar displacement peaked and began to relax, the ratio started to increase and approached a value of 1 at times over 200 seconds (corresponding to a distance of 4-7 μm from the edge). This indicated that talin cleavage at early adhesions was a transient event, which might explain why it was not previously detected in single-timepoint biochemical experiments and highlighted the importance of dynamic tracking. When we analyzed GFP-NC-talin-mCherry during the same phase of cell spreading, the talin rod to head ratio was relatively constant at a value close to 1 (Fig. 3d). Thus, the talin cleavage was limited to the very early adhesions under force; and after the peak in traction force, cleavage decreased.

To understand the change in the rate of recruitment of talin head and rod we fitted a linear curve through the respective molecule recruitment curves (Fig. 3b and 3e) for the two phases of pillar displacement (before maximal pillar displacement and after maximal pillar

displacement - before and after the grey bands in Fig. 3c and Fig. 3f). For WT-talin cells, the net rate of recruitment of talin head and rod were significantly different in both phases. While cells pulled on the pillars, talin head had a higher recruitment rate than the rod (Supplementary Fig. 4c). However, once the pillar reached maximal displacement and started to relax, the rate of recruitment of talin rod became higher than that of the head (Supplementary Fig. 4d). This change in relative rates of recruitment of talin head and rod was possible if after maximal substrate force, cleavage stopped and heads continued to dissociate while full-length molecules were recruited.

Supplementary Figure 4

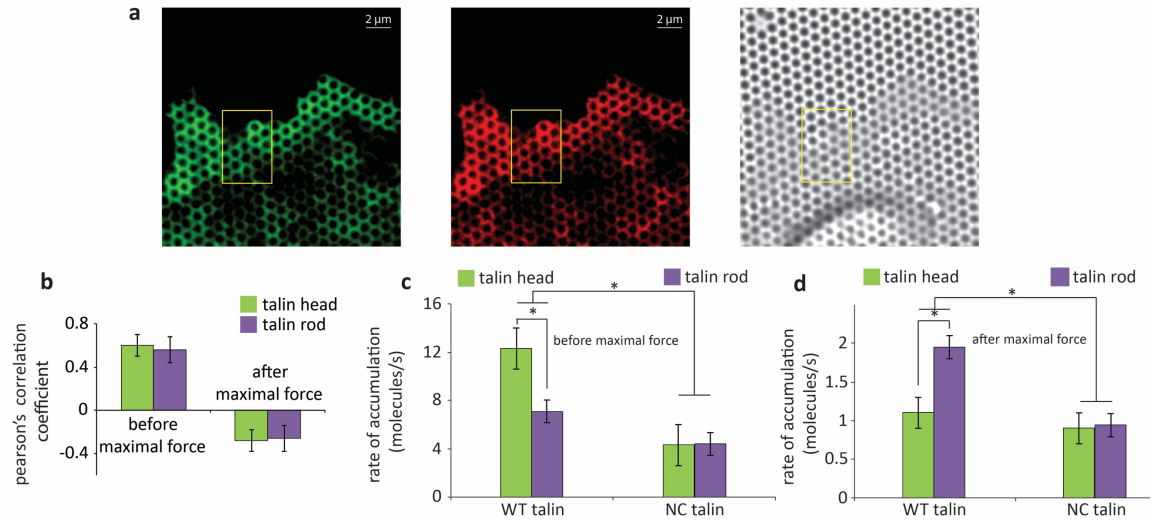

Supplementary Figure 4. Talin cleavage occurs when cell is pulling on the substrate. **a**, Images showing a spreading cell edge of cell expressing GFP-talin-mCherry. **b**, Pearson's correlation coefficient for pillars displacement and recruitment of talin head or rod molecules (as in correlation between curves from Fig. 3b and Fig. 3c). n>50 pillars, n>12 cells each. Talin head recruitment rate is higher than that of talin rod when force is being applied by cell and then rate of accumulation

of talin rod becomes greater than that of talin head **c** and **d**, Rate of accumulation of talin head and talin rod for WT and NC-talin cells.

In the case of NC-talin there was no difference in the recruitment rate of talin head or rod (Supplementary Fig. 4c,d). Interestingly, the rate of recruitment of molecules was low and similar to that of WT-talin cells after maximal pillar displacement (Supplementary Fig. 4c,d). This further supports the hypothesis that rapid talin cleavage occurred in the first phase of cell force development and that the rate of cleavage dropped dramatically once the cells pulled the substrate to maximum displacement.

Notably, for NC-talin, not only was the overall rate of recruitment of talin molecules slower than WT-talin, but also the overall rate of pillar movement (to reach the maximal displacement) was significantly lower than that with WT-talin (Fig. 3e,f,g, Supplementary Fig. 4c,d). This was due to frequent releases of the pillars during their displacements (arrows in Fig. 3f), which could have resulted from the breakage of integrin-talin-actin linkages[6,20]. This strongly indicated that talin cleavage was essential for proper adhesion development.

NC-talin increases early adhesion lifetime over full length talin, talin head or talin rod fragment leading to abnormally large and frequent adhesions.

In recent studies, we showed that early adhesions involved clusters of about 50 activated integrins in 100 nm circles that formed in a talin-dependent manner[23]. On glass, most of these clusters dissociated after about 2 minutes, but about 20% persisted and formed

adhesions. Since we and previous studies found that adhesions formed with NC-talin were larger than WT talin, we wondered whether these clusters of integrins were altered. In order to understand how NC-talin affected these initial steps of adhesion formation, we looked at integrin clustering using super-resolution microscopy (PALM) on supported lipid bilayers (SLB) of biotin-RGD (the ligand for integrins) that was freely diffusing (Fig. 4a).

The density of clusters (number of clusters per unit area) increased two-fold with NC-talin versus WT-talin (Fig. 4b), with a marginal increase in cluster diameter (Fig. 4c) fitting well with the idea of more frequent adhesion formation. Similarly, the integrin cluster density was higher than that of talin head, or talin rod fragment[23]. Further, the number of integrins in each cluster also increased by approximately 50 percent (Fig. 4d), indicating that talin cleavage was involved in regulating both the number of clusters and integrin packing in each cluster. Thus, NC-talin was activating and clustering integrins more than the other talin forms.

Since the clusters disassembled faster on glass, there was potentially a role for force in causing early adhesion disassembly that could have been inhibited by NC-talin. To test this we seeded cells expressing WT-talin and NC-talin on FN coated glass and looked at adhesion area per total cell area (Fig. 4e) during early cell spreading. For WT-talin cells,

Figure 4

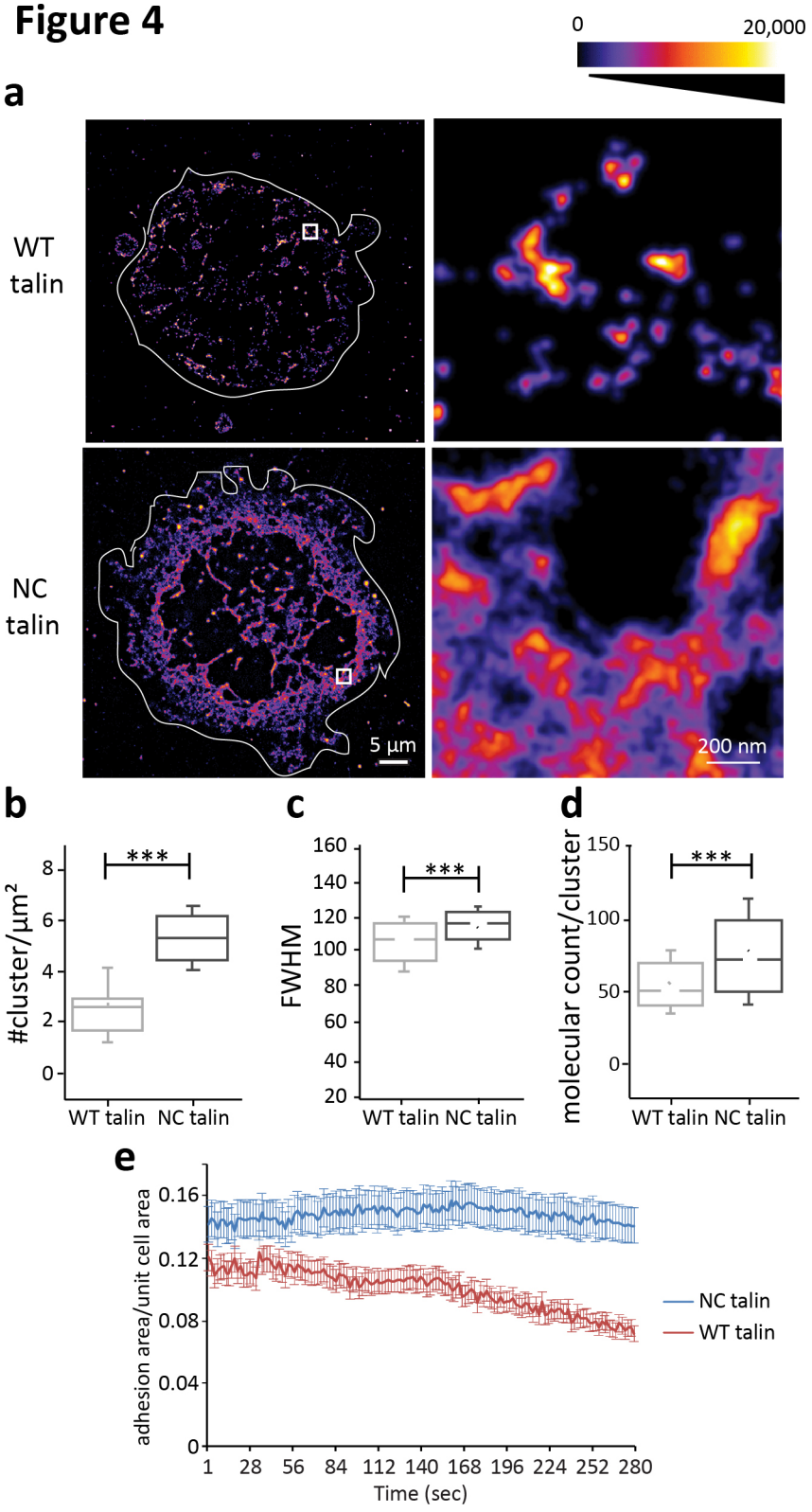

Fig. 4 Talin cleavage regulates the number of integrins at adhesion site. **a**, GFP tagged constructs of WT-talin or NC-talin were expressed in Talin1$^{-/-}$ MEFs and cells were spread on SLBs for 15 minutes and imaged using PALM. The imaged entity is Avidin-RGD. The bar indicates increasing density of RGD molecules within the cluster measured by PALM. White line marks the cell boundary and the rectangle region is the zoom-in region in the right panel. **b,c,d** Box plots show comparative distributions of number of molecules per cluster, Full Width Half Maximum (FWHM) of the clusters, and the number of clusters per µm^2 of the cell area, with the horizontal lines representing the medians and the whiskers representing SDs. (WT-

talin: 7746 clusters from 11 cells; NC-talin: 8614 clusters from 9 cells). In the case of NC-talin, the number of molecules increased from an average of 50 to 74.5, and the density of clusters increased from 2.7 per μm^2 to 5.3 per μm^2 (***$p<0.001$). However, the cluster size (FWHM) only increased marginally from 107 to 118 nm. **e**, Ratio of adhesion area to total cell area for WT- or NC-talin cells during early spreading on glass. Cells were seeded on FN coated glass and then imaged every few seconds through TIRF microscopy. n>5 for each case in **e**.

as cells spread, this ratio decreased whereas for NC-talin cells it increased or stayed constant, indicating that more adhesions persisted with NC-talin and adhesion turnover was significantly decreased. This strongly indicated that NC-talin inhibited force-dependent early adhesion disassembly. We hypothesized that force affected talin cleavage and played a role in regulating adhesion formation.

Talin dynamics in adhesions is regulated by actomyosin force dependent talin cleavage

Previous studies showed that regulation of integrin adhesions was an extremely dynamic process involving intricate interplay of forces and adhesion molecules[24,25]. In binding studies, the talin head bound to integrins almost six times more strongly than full length talin[26]. Therefore, we tested whether talin cleavage affected the kinetics of talin molecules in nascent adhesions. Using fluorescence recovery after photobleaching (FRAP) of both GFP and mCherry on pillar adhesions, we measured the recovery rate for both head and

rod. In particular, cells expressing GFP-talin-mCherry (wild-type or mutant) were seeded on 24 kPa rigidity pillars and a line of pillars perpendicular to the cell edge was bleached as the cell continued to spread (Fig. 5a). Fluorescence recovery for both GFP and mCherry was similar in the initial phase, indicating that talin was uncleaved when it bound to the adhesions (Supplementary Fig. 5a).

Supplementary Figure 5

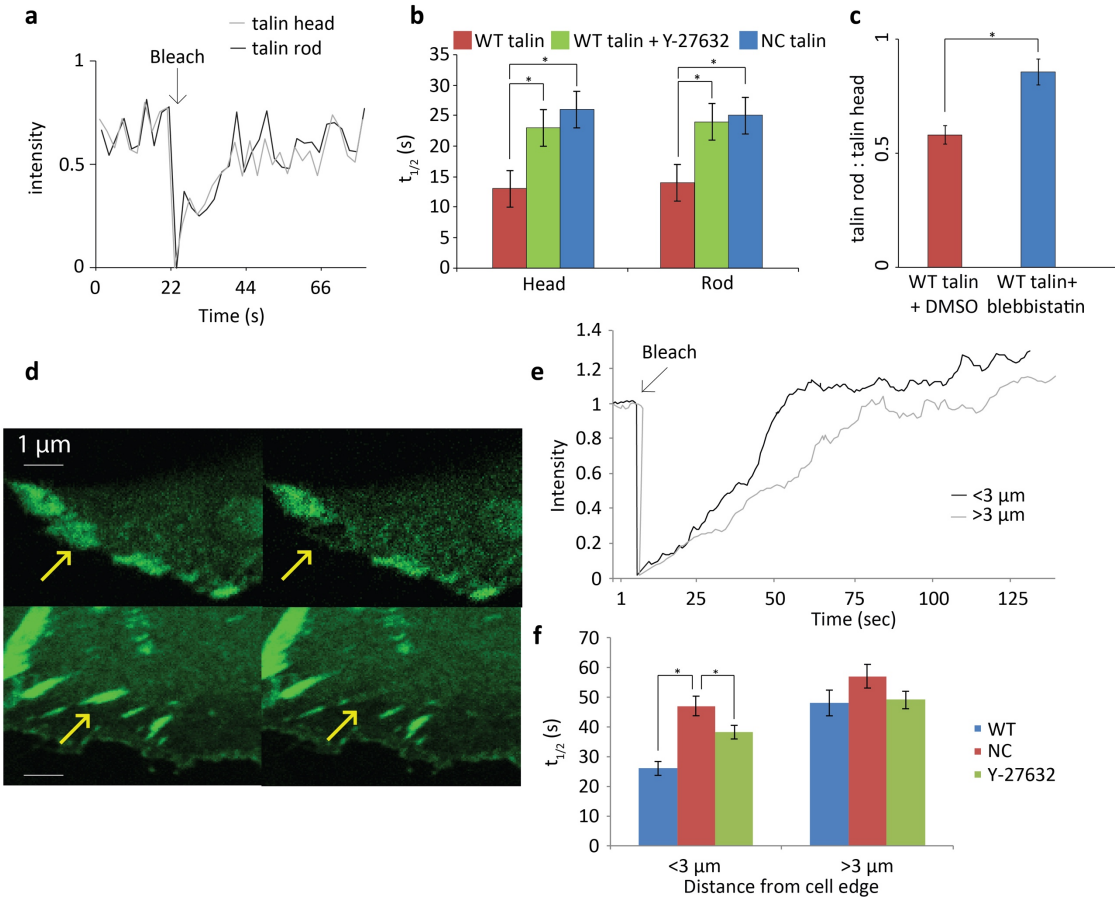

Supplementary Figure 5. Intact talin is recruited to early adhesions and force dependent talin cleavage alters talin dynamics in adhesions. **a**, Fluorescence recovery curves for talin head (GFP) or talin rod (mCherry) for a single pillar (pillar 2 as explained in Fig. 5). **b**, $\mathbf{t_{1/2}}$ of the recovery curves from panel **a** with or without actomyosin force inhibition by Y-27632. n>20 pillars, 12 cells. **c**, Ratio of talin rod to talin head (mCherry to GFP) for

individual adhesion sites (single pillars- pillar 2) with Blebbistatin or control (DMSO) in an experiment similar to that in Fig. 3. 31 pillars, 7 cells. **d**, Cells expressing double-tagged talin on glass before and after bleaching of their respective adhesions. These adhesions are at different perpendicular distance from the spreading cell edge. **e**, Fluorescence recovery curves for the bleached adhesions. **f**, Adhesions were grouped based on their perpendicular distance from the spreading edge (greater than or less than 3 μm). Then $\mathbf{t_{1/2}}$ of the recovery curves was calculated with or without actomyosin force inhibition by Y-27632. 16 cells.

It should be noted that this FRAP experiment was done on spreading cells where the bleached area was certainly not in steady state, which made the recovery curves appear non-ideal. This however did not affect the inference about talin dynamics. Fitting the recovery curves with a single exponential gave recovery half times of 13±3 and 14±3 s for GFP and mCherry, respectively (Supplementary Fig. 5b), indicating that WT-talin was recruited to bleached sites and cleavage occurred after recruitment. For pillars 4-7 microns from the edge, the half times of recovery increased to 26±3 and 27±4 s for GFP and

Figure 5

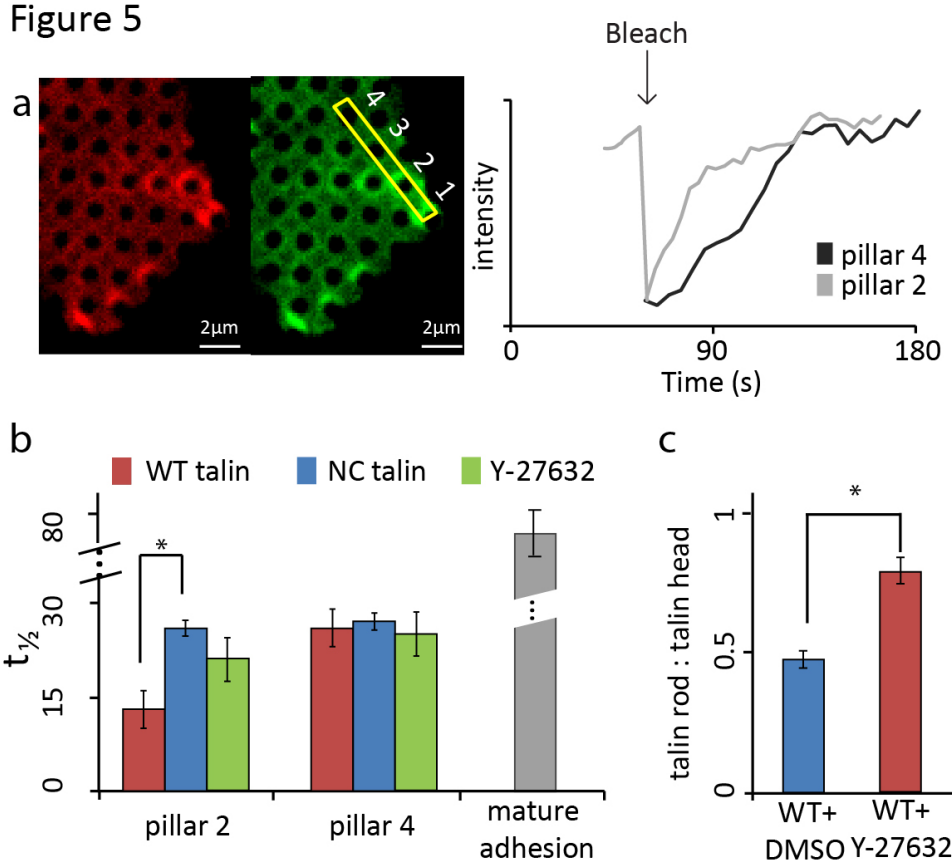

Fig. 5 Talin cleavage regulates nascent adhesion dynamics at force centres. **a**, Cell expressing double tagged WT- or NC- talin was allowed to spread on pillar arrays and then a line perpendicular to the cell edge was bleached (Yellow box). The recovery plots are for talin head (GFP) at single pillars in the bleached area (pillar 2 and pillar 4). **b**, Average $t_{1/2}$ for such recovery curves with WT- or NC-talin with or without the presence of Y-27632. n>8 cells for each case. $t_{1/2}$ for mature adhesions as measured in cells spreading on glass for >2 h is also shown. **c**, WT-talin rod to head ratio at the cell edge in the absence or presence of the ROCK inhibitor, Y-27632 in an experiment similar to that in Fig. 3.

mCherry, respectively (Fig. 5b), indicating much slower talin dynamics as the adhesions matured (further confirmation of this came from FRAP measurements on large adhesions in cells spreading for more than 2 h on glass that displayed a recovery half time of 76±9 s; Fig. 5b). On the other hand, with GFP-NC-talin-mCherry, the half-times for recovery were about 26±3 and 25±3 s irrespective of the distance from the leading edge (Fig. 5b, Supplementary Fig. 5b). These results supported the idea that talin cleavage altered talin dynamics in adhesions in a force dependent manner. This was confirmed when inhibition of actomyosin force by the ROCK inhibitor Y-27632 (20 μM) resulted in a significant increase in recovery half-time of WT-talin at the outer pillars (Fig. 5b, Supplementary Fig. 5b), similar to the case of NC-talin.

Talin cleavage was indeed reduced upon inhibition of traction force by Y-27632 addition since the mCherry/GFP ratio for pillars at the cell edge was nearly 1 (Fig. 5c; similar results were obtained in the presence of blebbistatin, Supplementary Fig. 5c). All of the evidence indicated that talin cleavage during the formation of adhesions was catalyzed by force and cleavage dramatically increased talin dynamics in early adhesions.

Talin rod, but not head, partially rescues cell growth and rigidity sensing in NC-talin cells

Since talin cleavage generated talin head and rod fragments that had downstream signaling functions independent of full length talin, we wondered if the fragments could rescue normal cell functions in NC-talin cells. Talin head affected focal adhesion turnover[27] and talin rod stimulated cell cycle progression[12]. To test their effects, we expressed mCherry-tagged talin head or talin rod fragments in GFP-NC-talin cells and allowed them to spread on FN coated pillars (24 kPa rigidity) while imaging them. As shown in Figure 6a, both

fragments localized to early adhesion sites and to mature adhesions.

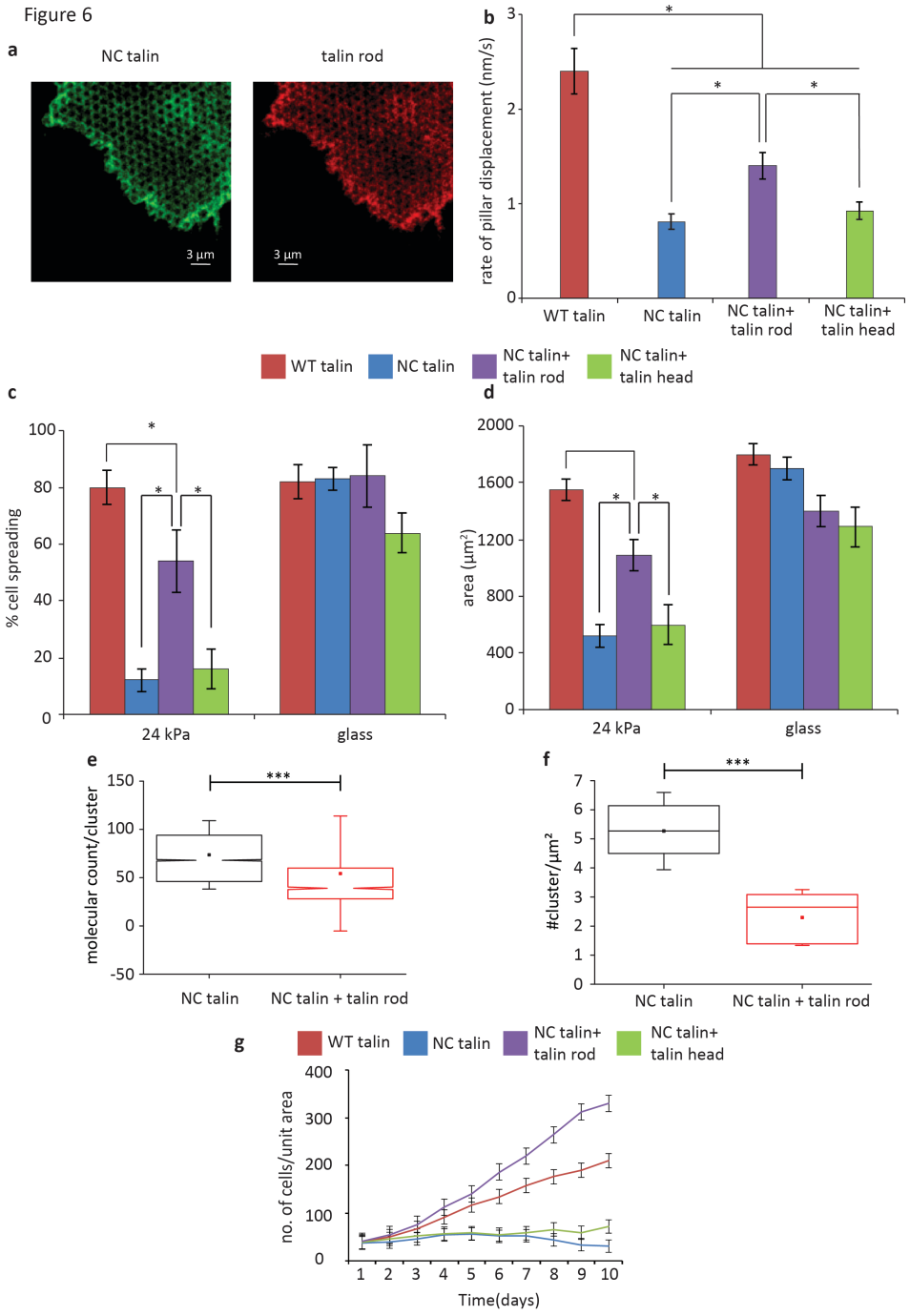

Fig. 6 Talin rod, but not talin head, can partially rescue cell spreading. **a**, Cells expressing GFP-NC-talin and mCherry talin rod on 24 kPa pillar array. **b**, Average rate of pillar displacement for cells expressing WT-talin, NC-talin, NC-talin and talin rod, NC-talin and

talin head. **c**, Percentage of spreading cells at 25 minutes on 24kPa pillars. **d**, Average whole cell area for cells detailed in panel **c**. **e,** Box plots showing comparative distribution of number of molecules per cluster for NC-talin cells and NC-talin cells with talin rod. **f**, Box plots showing comparative distribution of number of clusters per μm^2 for NC-talin cells and NC-talin cells with talin rod. The horizontal lines represent the medians and the whiskers representing SDs. (***$p<0.001$). 2438 clusters from 6 cells. **g**, Cell growth curves showing number of transfected cells per unit area for WT-cells, NC-talin cells, NC-talin cells with talin rod and NC-talin cells with talin head.

An early indication that rod fragments could restore normal functions came from measurements of the rate of traction force generation that was normally quite slow with NC-talin cells (Fig. 3f,g). Interestingly, expression of talin rod fragment enabled NC-talin cells to deform the substrate much faster, as shown by the increased pillar displacement rate (Fig. 6b); but still less than the rate with WT-talin cells. On the other hand, talin head had no significant effect on the rate of traction force development by NC-talin cells (Fig. 6b). Since the rod caused partial rescue of contractile activity, we tested if talin rod expression could restore normal cell spreading in NC-talin cells. Indeed, at 30 minutes, both the percentage of spreading cells and the cell spread area on 24 kPa pillars was partially restored and was significantly higher than with NC-talin cells (Fig. 6c,d). Again, talin head failed to have any such effect. To test if the talin rod fragment affected integrin density in early adhesions, we performed an experiment on SLBs similar to that shown in Figure 4, using cells co-expressing talin rod and NC-talin. Indeed, with talin rod, both the integrin density and number of integrin clusters were restored to that of normal WT talin

cells (Fig. 6e,f). These results strongly indicated that both the talin rod fragment and intact talin were important for normal cell adhesion development.

As a further test of the effect of talin rod expression, we measured the growth rate of NC-talin cells after rod expression. Surprisingly, with the talin rod, the growth rate of NC-talin cells was equal to that of the WT-talin cells but still less than the talin1-/- cells (Fig. 6g,h). In contrast, with the talin head, the growth rate of NC-talin cells was unaltered and their numbers decreased over time (Fig. 6g,h). Thus, we suggest that the talin rod fragment was needed even in the presence of uncleaved talin for growth, adhesion development and rigidity sensing.

Discussion

These studies document a number of abnormal behaviors of NC-talin cells: they 1) are inhibited for growth and EGF activation (Fig. 1), 2) have incorrectly formed integrin clusters (Fig. 4), and 3) fail to spread on intermediate rigidity substrates (Fig. 1). After cleavage, the talin rod releases from the adhesions more rapidly than talin head, which enables documentation of the sites where cleavage occurs (Fig. 2, Fig. 3). Since cleavage is blocked by myosin inhibition and occurs as traction forces are increasing, it appears that it is catalyzed by force in early adhesions. However, in mature adhesions, there is no evidence of cleavage. Although both the head and rod fragments could have functional roles, only the expression of the rod fragment in NC-talin cells partially rescues normal force generation, cell spreading, integrin density, and completely rescues cell growth (Fig. 6). Thus, we suggest that the cleavage of talin to generate the rod fragment is critical for normal cell behavior.

The inability of the NC-talin cells to grow is reminiscent of the findings with epithelial cells that did not grow without talin[26]. In the epithelial cells, the expression of the talin rod alone restored growth through a mechanism that involved the activation of FAK. Since the talin1-/- cells have talin2, they grow well but the expression of the NC-talin blocks proliferation potentially by displacing talin2 from adhesion sites. The talin rod fragment is binding to adhesion sites in the presence of NC-talin and there is no evidence of concentration of the fragment in other regions of the cell, including the nucleus (Fig. 6). Thus, it appears that the effect of talin rod is through an effect that it has on adhesion maturation. Because the rod fragment is less abundant at the adhesions than the head fragment, the role that it has there may be catalytic or it may be taking away inhibitory components from the adhesion. Much more research is needed to understand the surprising effect of the rod fragment in the presence of the NC-talin rod.

Rigidity sensing requires the proper assembly of the contractile units that occur primarily at early adhesion sites followed by proper contraction of those sites[20,28]. NC-talin cells appear to underestimate their substrate rigidity since a higher rigidity threshold is needed for NC-talin cell spreading. This indicates that the rigidity sensing process is compromised. In line with this, overall contraction of the pillars is much slower (Fig. 3g); and, the pattern of contractions indicates that there is slippage of pillar contacts during the contractions (arrows in Fig. 3f) which could be due to faulty reinforcement of talin-actin bond[6,25] under force. This indicates that the cleavage is needed for proper assembly of adhesive links from matrix to actin and for actin to support the force generation. As in the case of rod fragment stimulation of growth, the rod fragment increases the rate of force generation on adhesions.

Once again, this could be due to the displacement of an inhibitory component or the recruitment of molecules that can only bind to the rod in the absence of the head.

Talin's rapid turnover in early adhesions is surprising as it indicates that the adhesions are producing significant amounts of talin cleavage products. Although the heads are preferentially retained at the adhesions as indicated by higher GFP fluorescence levels, and consistent with in vitro binding studies[26], the heads are also turning over rapidly on the order of 10 s, especially at higher force locations (Fig. 5b). Both the rapid turnover and cleavage are dependent upon force and calpain activity, indicating that talin cleavage is the cause of the rapid turnover. In the absence of talin cleavage the turnover rate of talin is indeed slower than that when talin is cleaved (Fig. 5b). But even in the absence of talin cleavage, the turnover rate of talin in early adhesions is much more rapid than in later steady state adhesions (~25 vs ~75 s), which indicates that factors other than talin cleavage contribute to the lower stability of early adhesions. Nevertheless, the rapid dynamics of talin as a result of its cleavage in early adhesions appears to be needed for adhesion maturation and for cell growth.

There is a question of how activation of calpain occurs and two different activation mechanisms have been reported for calpain 2, either calcium entry or tyrosine phosphorylation[29–31]. Members of the transient receptor potential (TRP) family of channels have been previously shown to activate calpain by regulating Calcium ion influx[32,33]. TRPM4 channel is a mechanosensitive ion channel localized at adhesions[22] and in our experiments its inhibition reduces talin cleavage (Supplementary Fig. 2d). Therefore, there appears to be a role for calcium entry in calpain activation followed by talin cleavage. Measurements of the level of calcium in migrating cells show that there are no spikes in

the level of calcium[34]. However, several TRP family channels (TRPV4, TRPC1, TRPM4) are activated by forces applied to integrins in focal adhesions[22,32,35,36]. Low levels of calcium could enter locally and activate calpain, which could explain previous studies that show inhibition of motility upon inhibition of calcium channels[37,38]. It is reasonable to suggest that the TRP channels are able to locally release calcium at early adhesions as part of the maturation process.

Studies in the past have shown that talin head domain activates integrins more than full length WT-talin[26,39], but whether this activation is due to talin head or absence of talin rod is unclear. Since integrin clustering depends upon integrin activation, it is surprising that NC-talin causes larger clusters to form than does the head, rod[23] or wild type talin (Fig. 4). Integrin density can alter cellular perception of substrate rigidity and affect several critical processes[40,41]. However, free talin rod can restore normal density of integrins and cellular growth even in the presence of NC-talin (Fig. 6e,f,g,h). Thus, the size of the integrin clusters depends upon the presence of talin rod fragment from talin cleavage. Furthermore, talin rod restores cell spreading and substrate deformation to a large extent on 24kPa substrate in NC-talin cells (Fig. 6b,c,d). All of the evidence points to a significant role for the talin rod in adhesion maturation that is needed for a variety of functions leading to cell growth.

These results reveal an unexpected role of talin cleavage in regulating early adhesions that impact cellular mechanosensing, force generation and proliferation. Future studies could help elucidate the exact pathway(s) by which this cleavage is able to make both short- and long-term changes in cell behavior. Based on these results we suggest that talin cleavage and talin-mediated integrin activation might be two mechanisms that counter each other to

tightly regulate integrin density at adhesion sites. Disruption of talin cleavage can thus lead to the observed altered mechanosensing by changing integrin density. This altered integrin density in clusters can affect binding of adhesion partners like vinculin and α-actinin by altering talin stretching under force[25,42]. Indeed, the generation of force in the presence of NC-talin was much slower. Further, these results generally indicate that there is an additional step in the formation of focal adhesions[43] that requires the calpain-dependent cleavage of talin to release the talin rod.

Methods

Cell Culture, reagents, transfection and spreading experiments

Talin1 -/- cells from a previous study[44] were cultured at 37 °C in a 5% CO_2 incubator in Dulbecco's modified Eagle medium (DMEM) supplemented with 10% fetal bovine serum, 100 IU ml^{-1} penicillin–streptomycin, 2 μM L-glutamine (all reagents were from Thermo Fisher Scientific). Imaging experiments were conducted using starvation medium (unless otherwise mentioned) without phenol red or in Ringer's buffer (150 mM NaCl, 5 mM KCl, 1 mM $CaCl_2$, 1 mM $MgCl_2$, 20 mM Hepes, and 2 g/L glucose, pH 7.4). EGF (100 ng/ml, Thermo Fisher Scientific) was diluted into 0.5 ml medium before adding to the specimen. Cells were exposed to the following pharmacological inhibitors (Sigma-Aldrich unless otherwise mentioned) during spreading: ALLN (100 μM), 9-phenanthrol (10 μM), Y-27632 (20 μM, Calbiochem, Gibbstown, NJ), blebbistatin (50 μM).

Transfections were carried out 1 day before spreading experiments on sparsely plated cells (to avoid cell-cell interactions) using Lipofectamine (Thermo Fisher Scientific) according to the manufacturer's instructions, with 4 μg DNA. All constructs for NC-talin were a generous gift from Dr. David Critchley (University of Leicester).

Cells were trypsinized using TrypLE (Thermo Fisher Scientific) on the following day, centrifuged with growth medium, and then resuspended and pre-incubated in Ringer's buffer for 30 min before the experiment. Cells were then spread on the prepared substrate. We made sure that analysed cells were not interacting with other cells on the substrate.

Talin2 knockdown was performed using previously validated shRNA[23]. Cells were transfected with the shRNA using electroporation as per manufacturer's instructions.

Transfected cells were selected using antibiotic resistance (puromycin). Cells were used for experiments 72 hours after transfection.

EGF stimulation experiment

Cells transfected with WT- or NC- talin were serum starved for 30 minutes and then allowed to spread on glass for 6 hours with serum free media, after which they showed little to no membrane activity[45]. Cells were imaged for 5 minutes prior to addition of EGF (in 0.5 mL of media) and 10 minutes after. Cell edge kymographs were generated using ImageJ.

Analysis of Area

Cells were analysed using ImageJ to calculate area. To conservatively estimate the number of non-spreading cells we counted any cell forming a cell edge as spreading. One such spreading cell is shown in Fig. 1c and Supplementary Fig. 2a for each condition.

For area of focal adhesions we used Focal adhesion analysis server (FAAS)[46] with suitable parameters.

Cell growth analysis

Talin -/- cells were transfected with WT- or NC- talin using lipofectamine. Next day onwards, the number of spreading cells expressing GFP or mCherry (similar overall average intensity per pixel under identical imaging condition) in culture were counted for each case (plotted in Fig. 1a). This is a measure of cell proliferation as we can assume the uptake probability of the two plasmids (differing by a point mutation)[10] to be similar. We followed these cultures for 10 days.

Substrate preparation

Flat substrate fabrication and preparation

For 24 kPa substrate PDMS was prepared by using Sylgard 527 (part A : part B::1:1) with roughly ~6 percent Sylgard 184 (base : curing agent :: 10:1) and then spread on glass bottom dishes followed by incubation at 70 °C for 12 h in accordance to the previously developed methods[47]. The surfaces of the PDMS gels were coated with 10 μg/ml fibronectin for at least 1 hour prior to seeding cells. Previously, rigidity of the PDMS surfaces was measured by AFM indentation.

Pillar array fabrication and preparation

Pillar arrays (1.3 μm in height, 0.5 μm diameter, 1 μm centre to centre distance, k=8.4 nN/μm) were prepared as explained previously[19]. In short, Pillar bending stiffness, k, was calculated by Euler–Bernoulli beam theory:

$$k = \frac{3}{64}\pi E \frac{D^4}{L^3}$$

where D and L are the diameter and length of the pillar, respectively, and E is the Young's modulus of the material (PDMS). In this paper, pillar arrays have an effective modulus of 24.1 kPa which was calculated in accordance to the equation:

$$E\ (effective) = \frac{9}{4}\frac{k}{\pi A}$$

Where k is the bending modulus from Euler–Bernoulli beam theory and A is the contact area of the pillar with the cell[48]. 6-well plates with 0.2 kPa gels were bought from MuWells Inc. (San Diego, CA). All three substrates used in this study (soft gels, pillar arrays, or silanized cover glasses (incubated 2 h in 20% nitric acid, followed by exposure to gaseous

1,1,1,3,3,3-hexamethyldisilazane (Sigma)) were pre-coated with 10 μg/ml human plasma full-length pure fibronectin (Roche) for 1 h at 37 ℃.

Microscopy

Confocal microscopy was performed on a Zeiss LSM700 laser-scanning confocal microscope using a 100x N.A. 1.40 objective (Zeiss) maintained at 37 °C. Imaging for molecular counting experiments (Fig. 3) was done on an Olympus IX81 fluorescence microscope maintained at 37 °C with a 100× or 60 x N.A. 1.45 objective with or without additional 2x magnification and an electron-multiplying CCD camera (model Cascade-II:512, Photometrics), controlled by Micromanager software[49].

Molecule counting

Cells were seeded on prepared pillar tops and allowed to spread for 30 minutes (with or without the presence of pharmacological inhibitor) at which point they were fixed with 4% paraformaldehyde. Cells were then continuously imaged after focussing on pillar tops using an electron-multiplying CCD camera for mCherry and GFP. The acquired images were background subtracted using ImageJ. Then an intensity step size distribution analysis was done for the low intensity region of the bleaching curve (Fig. 2c, Supplementary Fig.3b,c). This identified the intensity step for a single fluorophore bleaching event. This process was done separately for both channels. Number of molecules was calculated by dividing pre-bleaching intensity by the step size. For live cell imaging (Fig. 3) we corrected the intensity for bleaching by using pillars far from the cell edge (>10 μm). Then we divided the corrected intensity by the step size established for GFP and mCherry to get a measure of relative number of molecules. All the imaging conditions from fixed cell molecular counting were maintained for live cell imaging. Since we were only comparing

mCherry and GFP, this relative number should not be affected by the switch in imaging condition (to live).

Pillar displacement measurement

Images acquired with either confocal imaging or bright field imaging were used as described previously to calculate pillar displacement[19,20]. In summary, cells were allowed to spread and pillar location was tracked using bright field illumination. Pillar position was tracked using nanotracking plugin of ImageJ[19,20].

Intensity normalization for TIRF imaging on glass using NC talin

A single image of cells expressing double tagged NC talin was taken before the continuous live cell imaging. The images were then background subtracted. Now the intensity distribution for each channel, within the adhesion, was observed. Since this is pre-bleaching image for NC-talin cells a normalization factor (NF) was calculated such that:

$$(\mathbf{I}_{red}/\mathbf{I}_{green}) * \mathbf{NF} = 1$$

NF was then averaged for multiple adhesions greater than 1 μm.

Now cells expressing cleavable double tagged talin were imaged in identical imaging conditions. Averaged NF was then used to normalize the red channel intensity as:

$$\mathbf{I}_{red\text{-}normalized} = (\mathbf{I}_{red}) * \mathbf{NF}$$

This $\mathbf{I}_{red\text{-}normalized}$ is essentially equivalent green channel intensity for $\mathbf{I}_{red}$. Once normalized both $\mathbf{I}_{green}$ and $\mathbf{I}_{red\text{-}normalized}$ are on the same intensity scale. These two intensities were then scaled together between 0 and 1 for ratio analysis (Supplementary Fig. 5).

FRAP experiment and analysis

Cells expressing WT- or NC- talin were serum starved and allowed to spread on prepared pillar arrays (with or without the presence of pharmacological inhibitor). Imaging was done at 37 °C using a confocal microscope with a 100x N.A 1.40 objective after focussing on pillar tops. Three channels - GFP, mCherry and TPMT- were simultaneously recorded at ~4 frames a second. While the leading edge was spreading, pillars were bleached in areas mentioned in Fig. 5 using fast bleach on Zeiss LSM 700. The images were then corrected for background using ImageJ. Single exponentials were then fitted to the recovery profiles in MATLAB and/or Excel to calculate half times ($t_{1/2}$).

For mature adhesions, cells were allowed to spread on glass (at room temp.) for 2 hours and then mature adhesions near cell edge were bleached using fast bleach on Zeiss LSM 700. Single exponentials were fitted after correction for background using ImageJ.

Assembly of Supported lipid bilayers

Lipids were purchased from Avanti Polar. 1,2- dioleoyl-sn-glycero-3-phosphocholine (DOPC) doped with 1,2-dipalmitoyl-sn-glycero-3- phosphoethanolamine-N-(cap biotinyl) (16:0 Biotinyl Cap PE) were used to assemble supported lipid bilayers. Detailed preparation methods were as previously described[50]. The supported lipid bilayers (SLBs) were then blocked with BSA for 30 min. Dylite650 labeled Neutravidin (from Invitrogen), linker between biotinyl-Cap-PE and biotinylated RGD, was incubated for 30minutes after washing. SLBs were then incubated with biotinylated RGD peptide for 30 minutes at room temperature. Cells were spread for 15 minutes at 37 °C and fixed using 4% formaldehyde for 10 minutes at 37 °C. This was followed by permeabilization with 0.5% Triton X 100 for 15minutes at 37 °C.

PALM imaging and Image processing

For photoactivated light microscopy (PALM), ~4 hours prior to imaging, the samples were incubated with 0.14μm multiflourophore beads (Spherotech, Cat no. FP0257-2) as fiducial markers. Just before imaging, the samples were placed in imaging buffer constituting of the following solutions with a volume ratio of 90:10:1 to deplete oxygen.

(1) 50 mM Tris-HCl (pH 8.0), 10 mM NaCl, 10% Glucose in PBS

(2) 1M mercaptoethylamine with pH adjusted to 8.5 using HCl

(3) Anti-bleaching oxygen scavenger system containing 14 mg Glucose Oxidase, 50 μl Catalase (17 mg/ml) in 200 μl 10mM Tris-HCl (pH 8.0), and 50mM NaCl DPBS solution.

Images for PALM were taken using a Zeiss Elyra microscope with a 100X objective (Alpha Plan Apochromat 100X oil NA 1.46) and an Andor iXon DU897 512x512 electron multiplier CCD camera. Dylite 650 was imaged with a very high power 647nm laser and at least 20,000 images were collected for each sample continuously with 50ms exposure for each frame. PALM images were reconstructed using maximum likelihood software written on the java platform[23]. Images were further analyzed using macros in ImageJ (NIH).

Statistics

All error bars are Standard Error of the Mean (SEM) unless otherwise mentioned. * represents rejection of null hypothesis at □□0.05 (p<0.05) in two tailed Student's t-test. Sample sizes and independent experiments are mentioned either in respective legend or relevant result text. Pearson's correlation coefficient was calculated in MATLAB. Live fluorophore intensity curves were filtered using a time average filter of 5-15 seconds in MATLAB or Excel.

References

1. Rozario, T. & DeSimone, D. W. The extracellular matrix in development and morphogenesis: a dynamic view. *Dev Biol* **341,** 126–40 (2010).
2. Schultz, G. S., Davidson, J. M., Kirsner, R. S., Bornstein, P. & Herman, I. M. Dynamic reciprocity in the wound microenvironment. *Wound Repair Regen. Off. Publ. Wound Heal. Soc. Eur. Tissue Repair Soc.* **19,** 134–148 (2011).
3. Desgrosellier, J. S. & Cheresh, D. A. Integrins in cancer: biological implications and therapeutic opportunities. *Nat Rev Cancer* **10,** 9–22 (2010).
4. Zhang, X. *et al.* Talin depletion reveals independence of initial cell spreading from integrin activation and traction. *Nat Cell Biol* **10,** 1062–8 (2008).
5. Ellis, S. J. *et al.* The Talin Head Domain Reinforces Integrin-Mediated Adhesion by Promoting Adhesion Complex Stability and Clustering. *PLOS Genet* **10,** e1004756 (2014).
6. Jiang, G., Giannone, G., Critchley, D. R., Fukumoto, E. & Sheetz, M. P. Two-piconewton slip bond between fibronectin and the cytoskeleton depends on talin. *Nature* **424,** 334–7 (2003).
7. Zaidel-Bar, R., Ballestrem, C., Kam, Z. & Geiger, B. Early molecular events in the assembly of matrix adhesions at the leading edge of migrating cells. *J Cell Sci* **116,** 4605–13 (2003).
8. Bachir, A. I. *et al.* Integrin-associated complexes form hierarchically with variable stoichiometry in nascent adhesions. *Curr Biol* **24,** 1845–53 (2014).
9. Yan, J., Yao, M., Goult, B. T. & Sheetz, M. P. Talin Dependent Mechanosensitivity of Cell Focal Adhesions. *Cell. Mol. Bioeng.* **8,** 151–159 (2015).

10. Franco, S. J. *et al.* Calpain-mediated proteolysis of talin regulates adhesion dynamics. *Nat. Cell Biol.* **6,** 977–983 (2004).

11. Bate, N. *et al.* Talin Contains A C-Terminal Calpain2 Cleavage Site Important In Focal Adhesion Dynamics. *PLOS ONE* **7,** e34461 (2012).

12. Wang, P., Ballestrem, C. & Streuli, C. H. The C terminus of talin links integrins to cell cycle progression. *J. Cell Biol.* **195,** 499–513 (2011).

13. Wang, H. B., Dembo, M. & Wang, Y. L. Substrate flexibility regulates growth and apoptosis of normal but not transformed cells. *Am J Physiol Cell Physiol* **279,** C1345-50 (2000).

14. Vogel, V. & Sheetz, M. P. Cell fate regulation by coupling mechanical cycles to biochemical signaling pathways. *Curr Opin Cell Biol* **21,** 38–46 (2009).

15. Eberwein, P. *et al.* Modulation of focal adhesion constituents and their down-stream events by EGF: On the cross-talk of integrins and growth factor receptors. *Biochim. Biophys. Acta BBA - Mol. Cell Res.* **1853,** 2183–2198 (2015).

16. Schneider, I. C., Hays, C. K. & Waterman, C. M. Epidermal Growth Factor–induced Contraction Regulates Paxillin Phosphorylation to Temporally Separate Traction Generation from De-adhesion. *Mol. Biol. Cell* **20,** 3155–3167 (2009).

17. Saxena, M. *et al.* EGFR and HER2 activate rigidity sensing only on rigid matrices. *Nat. Mater.* **advance online publication,** (2017).

18. Giannone, G. *et al.* Periodic lamellipodial contractions correlate with rearward actin waves. *Cell* **116,** 431–43 (2004).

19. Ghassemi, S. *et al.* Cells test substrate rigidity by local contractions on submicrometer pillars. *Proc Natl Acad Sci U A* **109,** 5328–33 (2012).

20. Wolfenson, H. *et al.* Tropomyosin controls sarcomere-like contractions for rigidity sensing and suppressing growth on soft matrices. *Nat Cell Biol* **18,** 33–42 (2016).

21. Meacci, G. *et al.* α-actinin links ECM rigidity sensing contractile units with periodic cell edge retractions. *Mol. Biol. Cell* mbc.E16-02-0107 (2016). doi:10.1091/mbc.E16-02-0107

22. Cáceres, M. *et al.* TRPM4 Is a Novel Component of the Adhesome Required for Focal Adhesion Disassembly, Migration and Contractility. *PLOS ONE* **10,** e0130540 (2015).

23. Changede, R., Xu, X., Margadant, F. & Sheetz, M. P. Nascent Integrin Adhesions Form on All Matrix Rigidities after Integrin Activation. *Dev Cell* **35,** 614–21 (2015).

24. Galbraith, C. G., Yamada, K. M. & Sheetz, M. P. The relationship between force and focal complex development. *J Cell Biol* **159,** 695–705 (2002).

25. Wolfenson, H., Bershadsky, A., Henis, Y. I. & Geiger, B. Actomyosin-generated tension controls the molecular kinetics of focal adhesions. *J Cell Sci* **124,** 1425–32 (2011).

26. Yan, B., Calderwood, D. A., Yaspan, B. & Ginsberg, M. H. Calpain Cleavage Promotes Talin Binding to the β3Integrin Cytoplasmic Domain. *J. Biol. Chem.* **276,** 28164–28170 (2001).

27. Huang, C. *et al.* Talin phosphorylation by Cdk5 regulates Smurf1-mediated talin head ubiquitylation and cell migration. *Nat. Cell Biol.* **11,** 624–630 (2009).

28. Yang, B. *et al.* Mechanosensing Controlled Directly by Tyrosine Kinases. *Nano Lett.* **16,** 5951–5961 (2016).

29. Khorchid, A. & Ikura, M. How calpain is activated by calcium. *Nat. Struct. Mol. Biol.* **9,** 239–241 (2002).

30. Franco, S. J. & Huttenlocher, A. Regulating cell migration: calpains make the cut. *J. Cell Sci.* **118,** 3829–3838 (2005).

31. Zanou, N., Louis, M., Schoor, M. V. & Gailly, P. Calcium entry through TRPC1 channels induces calpain activation and controls myoblasts migration. *Proc. Physiol. Soc.* **Proc Physiol Soc 14,** (2009).

32. Kerstein, P. C. *et al.* Mechanosensitive TRPC1 Channels Promote Calpain Proteolysis of Talin to Regulate Spinal Axon Outgrowth. *J. Neurosci.* **33,** 273–285 (2013).

33. Su, L. T. *et al.* TRPM7 regulates cell adhesion by controlling the calcium-dependent protease calpain. *J Biol Chem* **281,** 11260–70 (2006).

34. Tsai, F.-C. *et al.* A polarized Ca2+, diacylglycerol, and STIM1 signaling system regulates directed cell migration. *Nat. Cell Biol.* **16,** 133–144 (2014).

35. Matthews, B. D. *et al.* Ultra-rapid activation of TRPV4 ion channels by mechanical forces applied to cell surface β1 integrins. *Integr. Biol. Quant. Biosci. Nano Macro* **2,** 435–442 (2010).

36. Yang, Y., Gonzales, A. L., Sanders, L. & Earley, S. Membrane Stretch-Induced Activation of TRPM4 in Cerebral Artery Smooth Muscle Cells. *FASEB J.* **26,** 685.35-685.35 (2012).

37. Fiorio Pla, A. *et al.* TRPV4 mediates tumor-derived endothelial cell migration via arachidonic acid-activated actin remodeling. *Oncogene* **31,** 200–212 (2012).

38. Barbet, G. *et al.* The calcium-activated nonselective cation channel TRPM4 is essential for the migration but not the maturation of dendritic cells. *Nat. Immunol.* **9,** 1148–1156 (2008).

39. Cluzel, C. *et al.* The mechanisms and dynamics of avb3 integrin clustering in living cells. *J Cell Biol* **171,** 383–92 (2005).

40. Cavalcanti-Adam, E. A. *et al.* Lateral spacing of integrin ligands influences cell spreading and focal adhesion assembly. *Eur J Cell Biol* **85,** 219–24 (2006).

41. Cavalcanti-Adam, E. A. *et al.* Cell spreading and focal adhesion dynamics are regulated by spacing of integrin ligands. *Biophys J* **92,** 2964–74 (2007).

42. del Rio, A. *et al.* Stretching single talin rod molecules activates vinculin binding. *Science* **323,** 638–41 (2009).

43. Iskratsch, T., Wolfenson, H. & Sheetz, M. P. Appreciating force and shape-the rise of mechanotransduction in cell biology. *Nat Rev Mol Cell Biol* **15,** 825–33 (2014).

44. Priddle, H. *et al.* Disruption of the talin gene compromises focal adhesion assembly in undifferentiated but not differentiated embryonic stem cells. *J. Cell Biol.* **142,** 1121–1133 (1998).

45. Saxena, M. *et al.* EGFR and HER2 activate rigidity sensing on rigid matrices. *Nat. Mater.* (2017). doi:10.1038/nmat4893

46. Berginski, M. E. & Gomez, S. M. The Focal Adhesion Analysis Server: a web tool for analyzing focal adhesion dynamics. *F1000Research* **2,** 68 (2013).

47. Palchesko, R. N., Zhang, L., Sun, Y. & Feinberg, A. W. Development of polydimethylsiloxane substrates with tunable elastic modulus to study cell mechanobiology in muscle and nerve. *PLoS One* **7,** e51499 (2012).

48. Ghibaudo, M. *et al.* Traction forces and rigidity sensing regulate cell functions. *Soft Matter* **4,** 1836–1843 (2008).

49. Edelstein, A., Amodaj, N., Hoover, K., Vale, R. & Stuurman, N. Computer control of microscopes using microManager. *Curr Protoc Mol Biol 92* 14.20.1–14.20.17 (2010). doi:10.1002/0471142727.mb1420s92

50. Yu, C. & Groves, J. T. Engineering supported membranes for cell biology. *Med. Biol. Eng. Comput.* **48,** 955–963 (2010).

Chapter 5

Conclusion and future direction

EGFR can be activated in a ligand dependent or independent manner and is involved in several cancers. Although the interaction between EGFR with integrins is well known, its effects on rigidity sensing have never been explored. In Chapter 3, we find a new and important role of EGFR in rigidity sensing. Interestingly, we find that EGFR activity is required for rigidity sensing on stiff substrates, and this involvement is reduced on softer substrates. That is, on rigid substrates EGFR is recruited to early adhesions in a Src Family Kinase (SFK) dependent manner and plays an important role in rigidity sensing by directly affecting contractile unit (CU) formation, which are important for rigidity sensing. However, we show that even this interaction between EGFR and adhesion is transient and the amount of EGFR in adhesions decreases as adhesions mature. This indicates that EGFR is involved in adhesion formation but not adhesion maintenance. Therefore, one possible mechanism of involvement of EGFR in rigidity sensing is that force applied on initial adhesions causes changes in adhesion proteins such as talin, and this change enables the recruitment of EGFR to be phosphorylated by SFKs. Once EGFR is phosphorylated, it can activate multiple downstream pathways (like PLC dependent activation of PKC) which in turn can upregulate actomyosin forces. This is a positive feedback loop which can, in cycles, recruit more EGFR to be phosphorylated by SFKs. When on soft substrates, due to lack of force, this force dependent change in adhesions might occur to a lesser extent and therefore adhesions might not be able to recruit EGFR.

In Chapter 4, we show that talin cleavage by calpain is a force dependent process occurring after talin is recruited in the adhesion and that this cleavage is a critical step in adhesion assembly, affecting both rigidity sensing and cell growth. When cells express non-

cleavable talin, cells underestimate substrate rigidity, have abnormal adhesions, and fail to generate the required forces to deform the substrate. Some of this abnormal cell activity could be rescued by expressing the talin rod fragment (but not the talin head fragment) in the presence of non-cleavable talin. Interestingly, during this rescue experiment, a significant portion of the expressed talin rod is residing at the adhesion site despite containing NC-talin, suggesting that the released talin rod fragment might directly interact with other players in the adhesion. This postulate is supported by the fact that the talin rod has well known integrin and actin binding sites.

We suggest a mechanism in which intact talin is recruited to the adhesion site during the early steps of integrin clustering and then under force this talin gets cleaved by activated calpain2. A fraction of the cleaved talin rod then leaves the adhesion site but some cleaved free talin rod still resides in the adhesion interacting with other adhesion molecules. This talin rod can now enable normal adhesion formation through proper force generation and other cell cycle progression pathways. This mechanism is in sync with the observation that on soft substrates, adhesions don't grow, and cell growth is inhibited – as on soft substrates the force is not enough for talin cleavage.

In Chapter 3 we also showed that on rigid substrates, exposure of cells to EGF results in drastically increased cell motility. However, in Chapter 4 we find that this EGF stimulation seems to disappear in the absence of talin cleavage, even on stiff substrates like glass.

In context of these findings, it is possible that this reported calpain mediated talin cleavage is the force dependent change that is required for EGFR to be recruited to the adhesions. Therefore, future studies exploring the interplay between talin cleavage and EGFR activity are needed to understand these early events in adhesion formation. Specifically,

experiments focusing on identifying the role of talin rod fragments both in and out of the adhesion site are required. Further understanding the nature of interaction between the talin rod and EGFR under force, with or without other adhesion proteins, will help establish the overlaying mechanism determining critical cellular behaviors like rigidity sensing and cell growth. On the other hand, the function of the free talin head in adhesions is unclear. It is possible that this fragment's presence in adhesions is an intermediate state to a larger process where it will be slowly removed from the adhesion with other inhibitory factors, thereby again regulating cell viability.